PLOS ONE

RESEARCH ARTICLE

Building the cytokinetic contractile ring in an early embryo: Initiation as clusters of myosin II, anillin and septin, and visualization of a septin filament network

Chelsea Garno[1,2], Zoe H. Irons[2,3], Courtney M. Gamache[2,3], Quenelle McKim[2,3], Gabriela Reyes[1,2], Xufeng Wu[4], Charles B. Shuster[1,2], John H. Henson[2,3]*

1 Department of Biology, New Mexico State University, Las Cruces, New Mexico, United States of America, **2** Friday Harbor Laboratories, University of Washington, Friday Harbor, Washington, United States of America, **3** Department of Biology, Dickinson College, Carlisle, Pennsylvania, United States of America, **4** National Heart, Lung, and Blood Institute, National Institutes of Health, Bethesda, Maryland, United States of America

* henson@dickinson.edu

Citation: Garno C, Irons ZH, Gamache CM, McKim Q, Reyes G, Wu X, et al. (2021) Building the cytokinetic contractile ring in an early embryo: Initiation as clusters of myosin II, anillin and septin, and visualization of a septin filament network. PLoS ONE 16(12): e0252845. https://doi.org/10.1371/journal.pone.0252845

Editor: Claude Prigent, Centre de Recherche en Biologie cellulaire de Montpellier, FRANCE

Received: May 20, 2021

Accepted: November 24, 2021

Published: December 28, 2021

Data Availability Statement: The data are all contained in the paper and/or Supporting Information files.

Funding: This research was supported by National Science Foundation (www.nsf.gov) collaborative research grants to J. H. H. (MCB-1917976) and C. B. S. (MCB-1917983). C. G. was supported by the Charles Lambert Fellowship and the FHL Research Fellowship Endowment. The funders had no role in

Abstract

The cytokinetic contractile ring (CR) was first described some 50 years ago, however our understanding of the assembly and structure of the animal cell CR remains incomplete. We recently reported that mature CRs in sea urchin embryos contain myosin II mini-filaments organized into aligned concatenated arrays, and that in early CRs myosin II formed discrete clusters that transformed into the linearized structure over time. The present study extends our previous work by addressing the hypothesis that these myosin II clusters also contain the crucial scaffolding proteins anillin and septin, known to help link actin, myosin II, RhoA, and the membrane during cytokinesis. Super-resolution imaging of cortices from dividing embryos indicates that within each cluster, anillin and septin2 occupy a centralized position relative to the myosin II mini-filaments. As CR formation progresses, the myosin II, septin and anillin containing clusters enlarge and coalesce into patchy and faintly linear patterns. Our super-resolution images provide the initial visualization of anillin and septin nanostructure within an animal cell CR, including evidence of a septin filament-like network. Furthermore, Latrunculin-treated embryos indicated that the localization of septin or anillin to the myosin II clusters in the early CR was not dependent on actin filaments. These results highlight the structural progression of the CR in sea urchin embryos from an array of clusters to a linearized purse string, the association of anillin and septin with this process, and provide the visualization of an apparent septin filament network with the CR structure of an animal cell.

study design, data collection and analysis, decision to publish, or preparation of the manuscript.

Competing interests: The authors have declared that no competing interests exist.

Introduction

The process of cytokinesis is arguably the most essential function of the actomyosin cytoskeleton in animal cells. Despite significant research efforts extending over decades, key mechanisms underlying the formation of the cytokinetic contractile ring (CR) remain poorly understood [1–4]. This is particularly the case in animal cells, whereas in fission and budding yeast the roles of various CR-associated proteins and their structures, interactions and mechanisms have been more extensively characterized, imaged and modeled [2,5–7].

Our knowledge of the CR traces back to early transmission electron microscopy (TEM) based studies performed by Schroeder [8–10] and others [11–13] that indicated that cytokinesis in animal cells was mediated by a circumferential ring of actin and putative non-muscle myosin II filaments. Many of these CR studies hypothesized that the organization of actin and myosin II facilitated a sliding filament-based "purse string contraction" mechanism for ring constriction. However, clear evidence of the exact architecture of the CR was lacking in these earlier works and only more recent studies employing super-resolution microscopy and head and tail-based labeling of myosin II filaments [14–16] have demonstrated that myosin II within the mature CR is organized into aligned arrays that are oriented appropriately for a purse string contraction mechanism. Our previous work also extended this to the TEM level in which we used platinum replicas of cortices isolated from dividing sea urchin embryos to show a purse-string consistent orientation of both actin and myosin II filaments [16].

This recent success in defining actin and myosin II organization in the mature animal cell CR does not discount the fact that many unanswered questions remain. For example, little is known about the pre-CR structure in animal cells, although our recent work [16] and other studies [17–22] suggest that the precursor of the CR consists of an array of myosin II-containing clusters. In fission yeast, nodes of myosin II (Myo2) contribute to the CR assembly [23–27] through a search-capture and pull mechanism [28] and the interesting possibility exists that the clusters present in animal cells correspond to evolutionarily derived structures [29]. However, there are a number of fundamental differences between the cell division mechanisms of yeast and those in animal cells, including yeast's intranuclear karyokinesis, the spatial regulation of septation, and the added complication of a cell wall during cytokinesis. Given the similarities between sea urchin CR actomyosin clusters and yeast cytokinetic nodes, we hypothesize that CR assembly in the sea urchin embryo derives from a combined mechanism of yeast node-like congression followed by actomyosin contraction-mediated organization of the linear arrays of actin and myosin II filaments present in the mature CR. It is important to note that although myosin II is required for cytokinesis in a wide variety of organisms, fundamental questions remain about the precise roles of myosin II motor activity versus actin cross-linking ability in the mediation of this process [22,30,31].

Uncertainty about the structure of the animal cell CR extends beyond the actomyosin organization to the architecture and dynamics of two major CR scaffold proteins: septin and anillin. In budding yeast, the formation of a ring of septin filaments is a crucial step in CR assembly [7,32] and septin is associated with the CR in animal cells where it is thought to serve as a potential scaffold between the membrane, anillin, myosin II, and actin [33,34]. However, no study to date has definitively demonstrated the higher order structural organization of septins in an animal cell CR. In budding yeast, the ultrastructural arrangement of septin filaments in the bud neck has been visualized [32], although the progressive reorganization of septin filament structure from a ring, to an hourglass and then finally to a double ring are thought to be separate from the actomyosin ring [7,32].

Another scaffold protein critical for cytokinesis is anillin [35], which has been demonstrated to serve as an integrating link between RhoA and the CR components actin, myosin II,

septin and formin in animal and yeast cells [2,36–42]. In fission yeast, the anillin analogue Mid1 is essential for the initiation of the nodes which assemble into the CR [2,23,24]. However, similar to the case with septin filaments, little is known about the nanostructural organization of anillin in the animal cell CR. This fundamental uncertainty about the precise structure, function and dynamics of the two major cytokinetic scaffolding proteins argues that further work is needed to understand the complex organization of the animal cell CR [1,3,29].

Echinoderm embryos have long served as a crucial experimental model for cytokinesis research and have been used to demonstrate the existence of the CR [9], the essential role for myosin II in CR contraction [43], and the involvement of RhoA in the regulation of cytokinesis [44,45]. The sea urchin embryo also affords an approach crucial to the investigation of the 3D arrangement of ring constituents where CRs of early embryos can be isolated by adhering dividing embryos to coverslips, and then applying a stream of buffer [46]. The CRs in these isolated cortical preparations from first division embryos are roughly 10X larger than CRs in cultured mammalian cells and therefore overcome the significant limitation of small cell size and membrane curvature that plague studies trying to resolve the structure of the CR in mammalian cells. The cortex isolation method also allows for visualization of the CR from the vantage point of the cytoplasmic face of the plasma membrane. Multiple investigators have used isolated sea urchin embryo cortices to examine CR structure [47–50] including our own recent work [16].

In the present study we employ first division sea urchin embryos to investigate the structure and dynamics of the CR components actomyosin, septin2 and anillin. We extend our previous work by testing the hypothesis that the CR scaffolding proteins anillin and septin mirror the transformation of structural organization we have reported for CR myosin II [16]. We start by characterizing antibody probes for anillin and septin2 and then investigate their localization in the CR relative to myosin II via super-resolution imaging. Our results indicate that septin2 and anillin are affiliated with myosin II in the band of clusters/nodes that appears to serve as a precursor to the CR early in the cell division process. Within each cluster, anillin and septin2 both occupy a more central position relative to the myosin II minifilament head groups. As CR formation progresses, the septin2 and anillin staining focus into a narrower pattern coincident with a similar change in activated myosin II minifilament distribution. Both 3D SIM and STED imaging suggest the existence of a network of septin filaments affiliated with myosin II in mature CRs. Furthermore, the localization of either septin2 or anillin to the early CR myosin II clusters was not dependent on actin filaments given that it occurred in embryos treated with Latrunculin prior to cell division. Taken together these results underscore the structural evolution of the CR in sea urchin embryos from an array of clusters to a linearized purse string, the potential scaffolding roles that anillin and septin play based on their localizations with expected binding partners, and provide the visualization of an apparent septin filament network in the CR of an animal cell.

Materials and methods

Animals, cell lines, antibodies, and reagents

Lytechinus pictus sea urchins were purchased from Marinus Scientific (Lakewood, CA) and *Strongylocentrotus purpuratus* sea urchins were collected from Slip Point, a wave-exposed intertidal site in Clallam Bay, WA, USA (48.26260, -124.2532), with the sea urchins maintained in subtidal cages year-round at University of Washington Friday Harbor Laboratories (Friday Harbor, WA) and fed ad libitum with drift kelp (mainly blades of *Nereocystis luetkeana*). The animals in these *S. purpuratus* lab colonies are mixtures of sea urchins collected over several years under a series of Washington Department of Fish and Wildlife-approved scientific

collecting permits. Prior to spawning all sea urchins were kept in either running natural sea water or closed artificial sea water systems at 10–15˚C. LLC-PK1, a porcine kidney epithelial cell line, was obtained from American Type Culture Collection (Manassas, VA) and cultured according to the methods of Beach et al. [14].

Primary antibodies used included a rabbit polyclonal antibody raised against sea urchin egg myosin II heavy chain isolated via ATP-based precipitation of actomyosin from *S. purpuratus* egg extracts and electrophoretically purified [51], a mouse monoclonal antibody against the Ser19 phosphorylated form of myosin II regulatory light chain (P-MyoRLC) from Cell Signaling Technology (Danvers, MA), a rabbit monoclonal antibody against a peptide from human septin 2 from Abcam, Inc (Cambridge, MA), a mouse monoclonal antibody against a conserved epitope of chicken gizzard actin (clone C4) from EMD, Millipore (Burlington, MA), a rat monoclonal antibody against yeast alpha-tubulin (clone YL1/2) from Thermo Fisher Scientific (Pittsburgh, PA), and a mouse monoclonal antibody against human RhoA/B/C (clone 55) from Upstate Biotechnology (Lake Placid, NY). In order to generate a sea urchin anillin antibody, the PH domain of *S. purpuratus* anillin (aa 980–1124, Accession #XM_030975862) was cloned into pET302, expressed in *E. coli*, and the purified polypeptide used as the immunogen for a commercially prepared rabbit polyclonal antiserum (Thermo Fisher Scientific) and then affinity purified using the anillin PH domain. Appropriate secondary antibodies conjugated to Alexa Fluor 488, 555, 568, or Oregon Green as well as Alexa Fluor 488, 633, and 647 conjugated phalloidin were obtained from Thermo Fisher Scientific. Latrunculin A and B (LatA; LatB) were obtained from Cayman Chemical (Ann Arbor MI). Unless otherwise indicated, the majority of reagents were purchased from either Sigma-Aldrich (St. Louis, MO) or Thermo Fisher Scientific.

Gamete and coelomocyte collection, fertilization, and cleavage cortex isolation

Sea urchin gametes were collected via intracoelomic injection with 0.5 M KCl, with sperm collected dry and eggs spawned in either natural sea water or MBL artificial sea water (ASW: 423 mM NaCl, 9 mM KCl, 9.27 mM $CaCl_2$, 22.94 mM $MgCl_2$, 25.5 mM $MgSO_4$, 2.14 mM $NaHCO_3$, pH 8.0) and subsequently dejellied by multiple washing with ASW. Eggs were fertilized by addition of dilute sperm, the fertilization envelopes removed using 1 M urea (pH 8.0), and then washed into and reared in MBL calcium free sea water (MBL ASW minus $CaCl_2$ and plus 1 mM EGTA) at 10–15˚C. For disruption of actin filaments embryos were treated with either 1 μM LatA or 20 μM LatB starting at 30–60 min prior to first division. Cleavage cortices were generated as described in Henson et al. [46]. In brief, embryos at the appropriate stage of cell division were allowed to quickly settle onto poly-L-lysine (2 mg/ml) coated coverslips and then exposed to fluid shear force from a pipette containing an isotonic cortex isolation buffer (CIB: 0.8 M mannitol, 5 mM $MgCl_2$, 10 mM EGTA, 100 mM HEPES, pH 7.4). Isolated cortices were rinsed twice in CIB prior to further processing for fluorescent staining. Sea urchin coelomocytes were isolated from the perivisceral fluid of adult animals and maintained in coelomocyte culture media (0.5 M NaCl, 5 mM $MgCl_2$, 1 mM EGTA, and 20 mM HEPES, pH 7.2) as described in Smith et al. [52].

Fixation, fluorescent staining and microscopic imaging and analysis

Embryos–either attached to poly-L-lysine coated coverslips or cultured in suspension–were fixed in Millonig's fixative (0.2 M NaH_2PO_4, 0.136 M NaCl, pH 7.0) containing 3.7% formaldehyde for 20 minutes, washed 3X and then left overnight in 0.1% Triton X-100 in phosphate buffered saline (PBST), and then blocked overnight in 3% BSA diluted in PBST. Isolated

cortices were fixed in 2–3% formaldehyde in CIB for 5 min followed by blocking in 2% goat serum and 1% BSA in PBS for at least 30 minutes. For immunolocalization of RhoA/B/C, cortices were fixed in 10% trichloroacetic acid following the methods of Yonemura et al. [53]. Coelomocytes were settled and fixed as described in Smith et al. [52]. Immunostaining of all samples was performed with appropriate primary and secondary antibodies diluted in blocking buffer with embryos typically being stained in each antibody step overnight whereas cortices and coelomocytes were stained for 1 hour in each stage. In preliminary double labeling experiments the rabbit anti-septin 2 and rabbit anti-anillin antibodies were directly fluorescently labeled using the Zenon rabbit IgG labeling kit from Molecular Probes (Eugene, OR) and staining performed following the manufacturer's instructions. Fluorescent phalloidin was added to the secondary antibody staining step. Samples for conventional and 3D structured illumination super-resolution microscopy (3D-SIM) were typically mounted in nonhardening Vectashield antifade mounting media (Vector Laboratories, Burlingame, CA) plus or minus DAPI prior to imaging. Samples for stimulated emission depletion (STED) super-resolution microscopy imaging were mounted in Prolong Diamond mounting media (Thermo Fisher).

Conventional epifluorescence microscopy of samples was performed on a Nikon (Tokyo, Japan) 80i microscope using either a 40X/0.75 NA Plan Fluorite or 60X/1.4 NA Plan Apo phase contrast objective lens with digital images captured using a Photometrics (Tuscon, AZ) CoolSnap Cf cooled CCD camera. Confocal microscopy was performed on either an Olympus (Tokyo, Japan) Fluoview 500 laser scanning confocal microscope using a 40X/1.15 NA UApo water immersion DIC objective lens, or an Andor Dragonfly 505 spinning disk confocal system (Oxford Instruments, Abingdon, UK) using either an Olympus 60X/1.3 NA silicone or a 100X/1.49 NA oil immersion objective lens. Spinning disk confocal digital images were acquired with an Andor Zyla 4.2 cMOS camera.

Super-resolution microscopy was performed using two different methods. For 3D-SIM [54] we utilized a DeltaVision OMX 3D-SIM Imaging System (GE Healthcare Bio-Sciences, Pittsburgh, PA) with an Olympus 60X/1.42 NA objective lens. Captured images were reconstructed using SoftWoRx software. STED super-resolution microscopy [55] was performed on a Leica (Wetzlar, Germany) Sp8 STED confocal microscope using a 100X/1.4 NA objective lens.

For all forms of microscopic images, processing and analysis was performed using either Fiji/ImageJ (Bethesda, MD) or Bitplane Imaris (version 8.1–9.1.2; Andor). Graphs were prepared and statistical analysis carried out using GraphPad Prism 8 (San Diego, CA), with box and whisker plots having the following attributes: the box extends from the 25th to the 75th percentiles, the whiskers extend to the minimum and maximum values, and the line in the middle of the box is the median. Final figures were prepared using Adobe Photoshop (San Jose, CA).

Gel sample lysates and immunoblotting

Gel sample lysates of either sea urchin egg/embryos or LLC-PK1 cells were generated by pelleting cells and then adding hot 2X sample buffer (625 mM Tris-HCl pH 6.8, 25% glycerol, 2% SDS, 0.01% bromophenol blue, 5% β-mercaptoethanol) at five times the volume of packed cells followed by boiling for 5 minutes. Gel samples were loaded into a 4–15% Mini-PROTEAN TGX precast protein gel (Bio-Rad, Hercules, CA) and transferred onto an Immobilon PDF membrane (Millipore) or nitrocellulose for probing. Total protein staining of nitrocellulose blots was performed using 0.1% Ponceau S in 5% acetic acid. Blocking and antibody incubation was performed in TBS-Tween supplemented with 5% instant milk. Bound antibody detection was performed for septin2 immunoblots using alkaline phosphatase conjugated

secondary antibodies and a BCIP+NBT substrate. For anillin immunoblots HRP conjugated secondary antibodies were used and detected by chemiluminescence using a Immun-Star HRP kit, with imaging performed on a ChemiDoc XRS molecular imaging system from Bio-Rad.

Results

Characterization of antibodies against the sea urchin anillin PH domain and septin2

Sea urchin anillin is predicted to contain the domains that confer anillin with its unique CR integration functions [42]. These include a N-terminal domain (NTD) with a formin binding site (FBD), nearby myosin II and actin binding domains (MBD and ABD), an anillin homology domain (AHD) which interacts with RhoA, and a C terminus pleckstrin homology (PH) domain which allows for binding with septin and membrane phospholipids (Fig 1A). The PH domain of *S. purpuratus* anillin was cloned and used to generate a rabbit polyclonal antiserum which was affinity purified against the recombinant anillin PH domain and its specificity confirmed by immunoblotting (Fig 1B). Rabbit anti-sea urchin anillin reacted with the purified recombinant 16 kDa anillin PH domain antigen, and with a ~120 kDa species in *S. purpuratus* egg and embryo lysates consistent with the predicted molecular mass of *S. purpuratus* anillin (Fig 1B).

Septins are a family of GTP-binding proteins that form filaments composed of linear arrays of hetero-oligomers of different isoforms which vary across species [33], and the sea urchin *S. purpuratus* genome has been shown to encode homologues of the human Sept2, Sept3, Sept6, and Sept7 subgroups [56]. Immunoblotting of a lysate of LLC-PK1 mammalian cells or *L. pictus* embryos with a commercial rabbit monoclonal antibody against a peptide antigen (between aa 1–100) from human Sept2 resulted in an immunoreactive band of ~45 kDa which is similar to the 42 kDa molecular mass of human Sept2 (Fig 1C).

The sea urchin anillin and septin2 antibodies were initially further characterized by testing for expected immunofluorescence staining patterns. Anillin proteins have a nuclear localization sequence (NLS) and have been shown to be localized in the nucleus during interphase in some species [35,36,57,58]. Sea urchin anillin has a weak putative NLS (aa 632–636, Fig 1A) and staining of newly fertilized, sperm aster stage embryos shortly following syngamy with the anti-sea urchin anillin antibody showed it was present within the zygote nucleus as well as in the cortex (Fig 1D–1G). Weak nuclear localization of anillin in interphase cells was also observed in isolated adult sea urchin coelomocytes that are terminally differentiated, post-mitotic cells (Fig 1H–1J). Septin filaments are known to localize in stress fibers in cultured cells [34] and in cilia and flagella [59]. Staining adult coelomocytes with the septin2 antibody showed clear localization in the stress fiber-like actomyosin bundles of large phagocytes and in the flagellar axonemes of vibratile cells (Fig 1K–1M).

Anillin and septin2 localize to the CR of whole embryos and isolated cleavage cortices

During first division of sea urchin embryos, overlapping microtubules from the asters deliver the centralspindlin/RhoGEF complex to the equator that activates RhoA [45,60,61], which in turn is thought to recruit anillin and activate CR actomyosin contraction. Dividing embryos stained for microtubules and anillin showed that the equatorial cortex accumulation of anillin–which was not apparent in late anaphase (Fig 2A–2C)–appeared coincident with the invagination of the cleavage furrow in early telophase (Fig 2D–2F). A similar concentration of

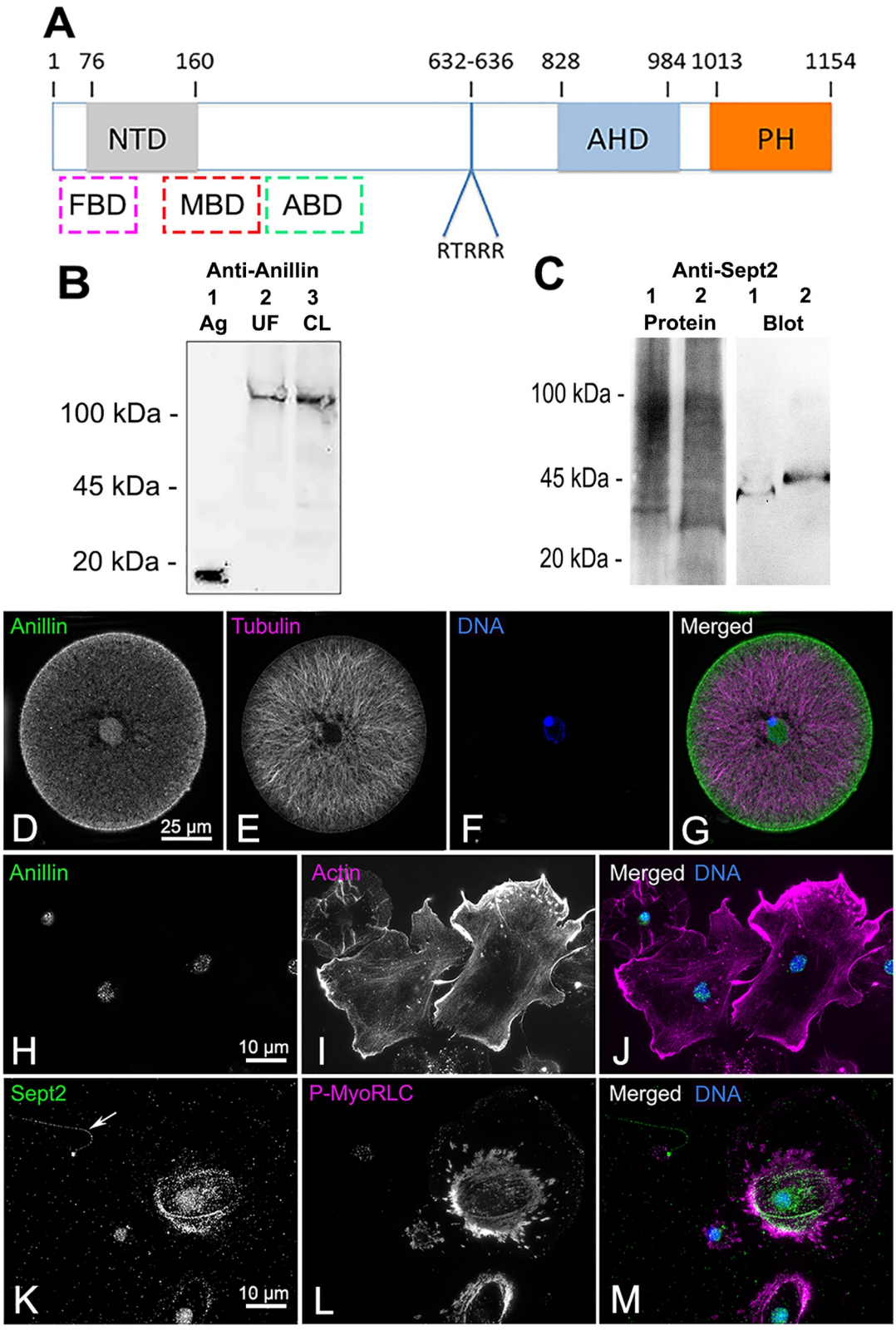

Fig 1. Characterization of antibodies against sea urchin anillin and septin2. (A) Starting at the N terminus, the predicted domains of sea urchin anillin include a formin binding domain (FBD), a N-terminal domain (NTD), a myosin II binding domain (MBD), an actin binding domain (ABD), a candidate nuclear localization sequence (RTRRR), an anillin homology

domain (AHD), and a plecstrin homology domain (PH). The dashed boxes for FBD, MBD, and ABD indicate approximate locations. (B) Immunoblot of affinity purified anti-sea urchin anillin PH domain antibody against the purified peptide antigen (Ag, lane 1) shows the expected 16 kDa immunoreactive band. Blotting this antibody against lysates of either unfertilized *S. purpuratus* eggs (UF, lane 2), or first cleavage embryos (CL, lane 3) reveals a ~120 kDa immunoreactive band. (C) Immunoblot of anti-human septin2 peptide antibody against LLC-PK1 cell lysate (lane 1 total protein left and immunobot right) and *L. pictus* first cleavage embryo lysate (lane 2 total protein left and immunoblot right) reveals a ~40–45 kDa immunoreactive species. (D-J) Anillin (green) staining of a *S. purpuratus* sperm aster stage early embryo (D-G) and adult coelomocytes (H-J) shows that anillin localizes to the nucleus and in early embryos to the cortical region. Embryos are co-labeled for microtubules (magenta) and DNA (blue), whereas coelomocytes are co-labeled for actin filaments (magenta) and DNA (blue). (K-M) Septin2 (green) staining of adult *S. purpuratus* coelomocytes also labeled for P-MyoRLC (magenta) and DNA (blue) demonstrates the expected staining of septin in stress fiber-like actomyosin bundles in phagocytes and in the flagella of vibratile cells (arrow in K).

https://doi.org/10.1371/journal.pone.0252845.g001

anillin staining in the cleavage furrow has been reported in many cell types [35,36,40,62], although broader cortical staining is often present throughout cell division, which is not seen in the sea urchin embryos. As cleavage furrow ingression progressed, anillin staining became highly concentrated in the CR region (Fig 2D–2O)–with off axis images showing a clear ring shaped anillin-stained structure (Fig 2J–2L)–and remained associated with the midbody after the CR had disassembled (Figs 2M–2O and S1).

The CR in fixed sea urchin embryos can be readily localized using antibodies against the Ser19 phosphorylated form of the myosin II regulatory light chain (P-MyoRLC) which is indicative of activated myosin II that is capable of actin-based contraction [16,20,60]. Localization of either septin2 or anillin with P-MyoRLC in whole embryos showed a clear association with the CR that began as a broad band of clusters (Fig 3A–3D and 3M–3P) which then concentrated into a narrow ring as furrowing progressed (Fig 3E–3H and 3Q–3T), and culminated in retention in the midbody (Fig 3I–3L).

Septin2 and anillin also localized with P-MyoRLC in the CR regions of cortices isolated from dividing embryos (Figs 4 and 5). In examining cortices from a time series of isolations over the course of cytokinesis, those from earlier time points tended to display a broad band of punctate clusters or nodes which contained septin2, anillin and P-MyoRLC (Figs 4A–4D, 4I–4L, and 5A–5D). Note that we are confident that the cortex isolation process itself does not induce these clusters as our imaging of whole embryos (Fig 3) and previously published work [20] have also indicated the presence of CR constituent clusters in the early stages of cytokinesis. Widefield imaging of the clusters in isolated cortices suggested an incomplete overlap between the localization of septin2 or anillin staining and that of P-MyoRLC. In cortices isolated in the mid to late stages of cytokinesis, the septin2, anillin and P-MyoRLC staining patterns (Fig 4E–4H and 4M–4Q) all appeared to have coalesced into a patchy and more linearized pattern that became very concentrated in the latest stage cortices (Fig 5E–5L). In preliminary experiments involving widefield imaging of isolated cortices double-labeled for septin2 and anillin using direct fluorescent labeling of these two primary rabbit antibodies, we have observed a general colocalization between these proteins in mid-late stage CR regions (S2 Fig).

Quantification of the myosin II staining patterns of 247 cortices from 3 separate experiments showed that in cortices isolated early in cytokinesis (Fig 4R) punctate cluster staining predominated in the CR region (70% of cortices with CRs; Fig 4T), whereas in cortices isolated in mid-late cytokinesis (Fig 4S) patchy/linear CR staining patterns were more prevalent (76% of total cortices with CRs; Fig 4T). Localization of filamentous actin in cortices using phalloidin indicated that it codistributed with the clusters in early stages (Fig 5A–5D) and the condensed CR patterns present in late stages (Fig 5E–5L), as well as staining the microvilli present in these cortices (Fig 5C, 5G and 5K). RhoA/B/C was also enriched in the CR region containing anillin (Fig 5M–5P), septin2, actin and myosin II.

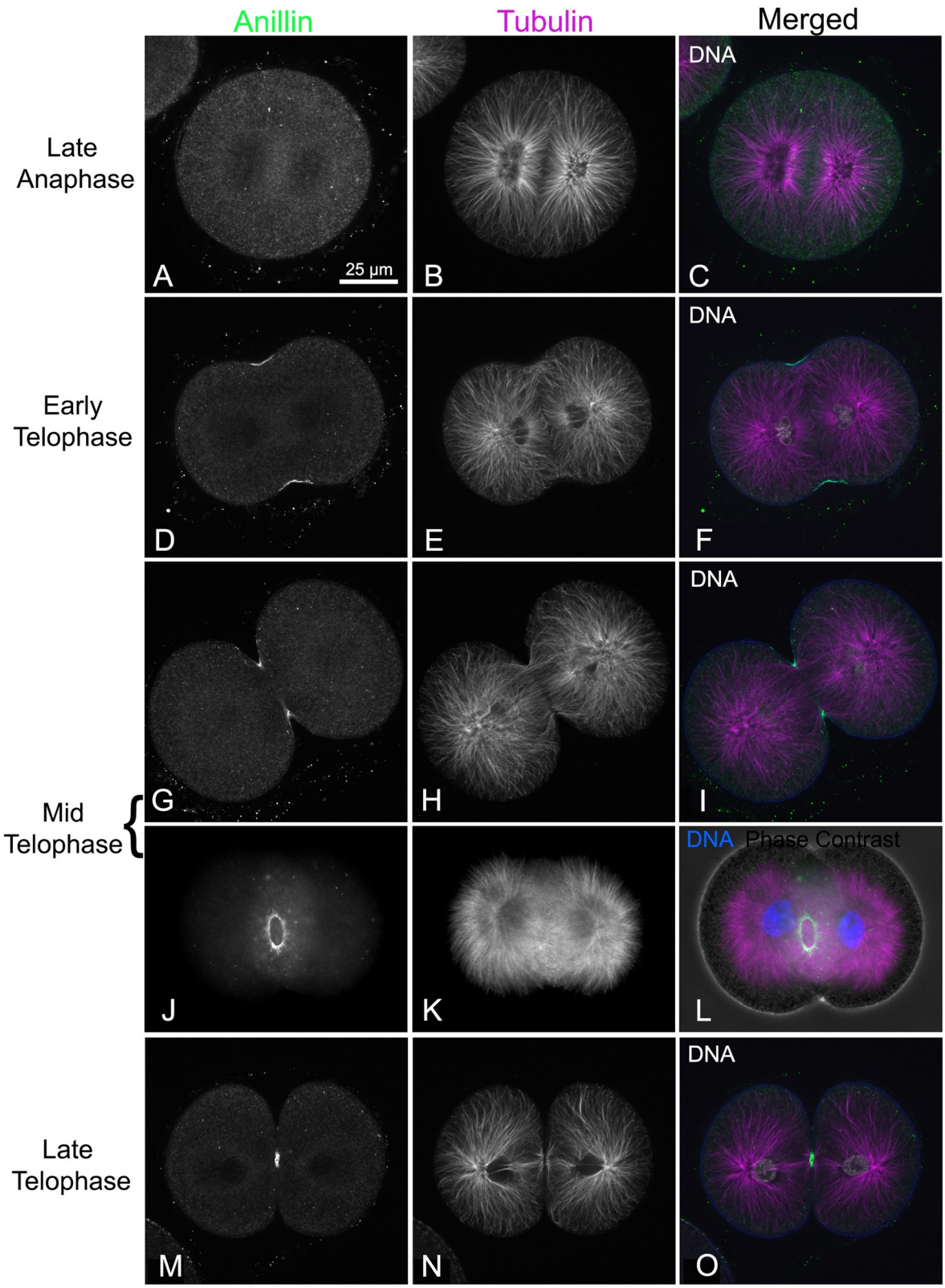

Fig 2. Anillin localizes to the cleavage furrow in first division embryos. In dividing *S. purpuratus* embryos co-labeled for microtubules (magenta) and DNA (white; blue in L) in order to determine mitotic progression, anillin (green) staining is not obvious in late anaphase

(A-C) but begins concentrating in the early cleavage furrow starting at the initiation of telophase (D-F) and continues through the midbody stage prior to abscission in late telophase (G-O). In off axis images the anillin staining appears as an entire ring similar to other CR markers (J-L). In L the phase contrast image is superimposed on the fluorescence image for context. The magnifications of A-O are equivalent and A-I plus M-O are confocal images whereas J-L are widefield images.

https://doi.org/10.1371/journal.pone.0252845.g002

Super-resolution microscopy reveals the organization of myosin II, anillin and septin2 clusters that serve as CR precursors

Consistent with our widefield imaging (Figs 4 and 5), 3D-SIM imaging of early cleavage stage cortices demonstrated that myosin II, septin2 and anillin are all organized in a broad band of regularly spaced clusters (Fig 6). Within these ring or stellate shaped clusters, the distribution

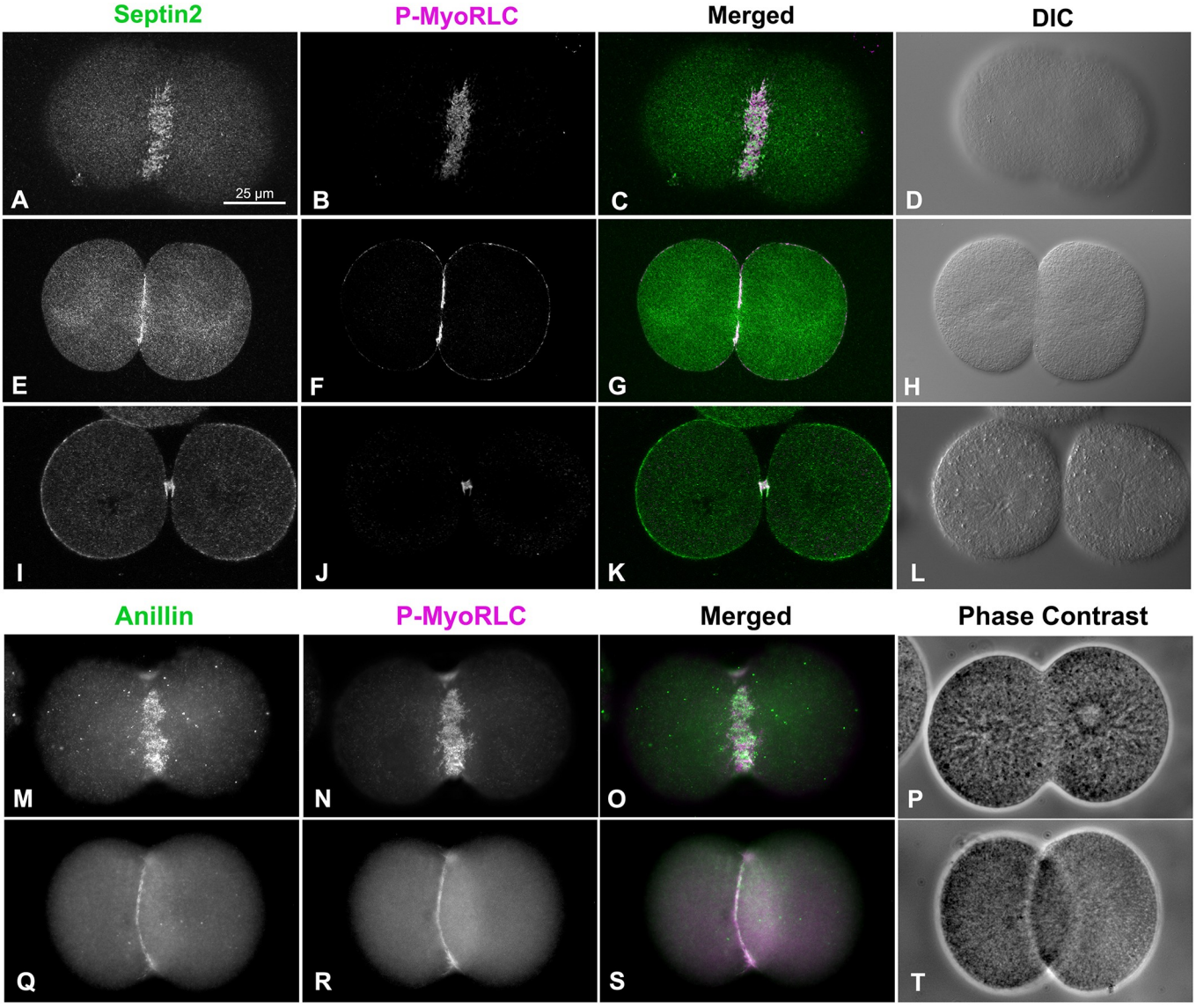

Fig 3. Septin2 and anillin colocalize with the CR marker P-MyoRLC in first division embryos. Both septin2 (A-L, green) and anillin (M-T, green) mirror P-MyoRLC (A-T, magenta) staining in dividing embryos and begin as collections of clusters (A-D, M-P) that progress to tight rings (E-H, Q-T), and end concentrated in the midbody (I-L). *L. pictus* embryos appear in confocal images in A-L, *S. purpuratus* embryos appear in widefield images in M-T, and the magnifications of A-T are equivalent.

https://doi.org/10.1371/journal.pone.0252845.g003

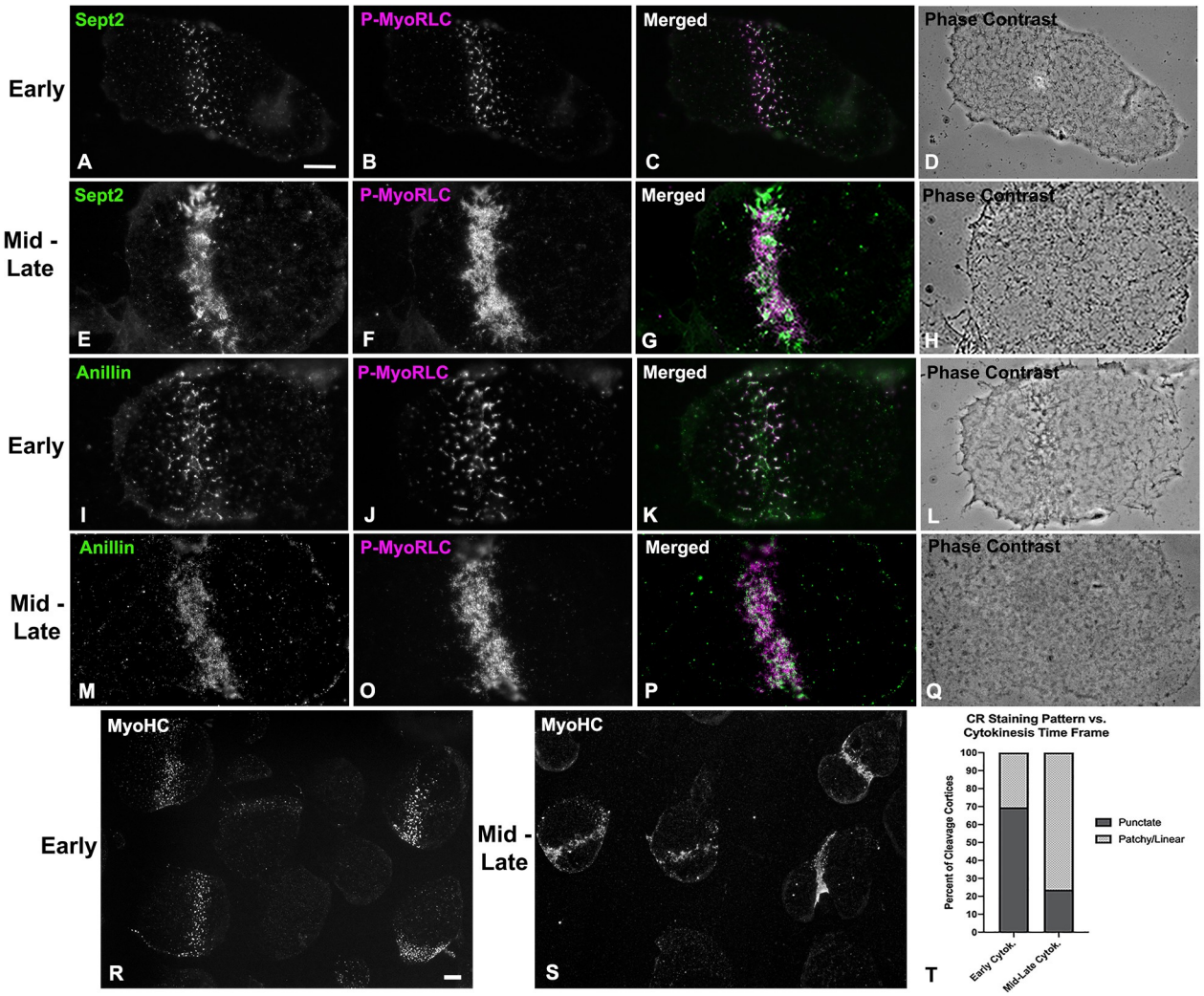

Fig 4. Widefield imaging of isolated cortices reveals that septin2 and anillin co-distribute with active myosin II and progress from clusters to more linearized arrays. Septin2, and active myosin II (P-MyoRLC) localize together in the CR regions of isolated cortices (A-H) and progress from regularly spaced clusters in early stages (A-D) to dense assemblages of more patchy and linear structures in late stages (E-H). Anillin displays a similar co-distribution with active myosin II, as well as the analogous evolution from clusters in early cortices (I-L) to denser and more filamentous arrays in mid-late cortices (M-Q). Lower magnification images of myosin II (MyoHC) staining in cortices isolated early in cytokinesis (R) shows the presence of punctate clusters in a majority of cortices containing CRs (percentages graphed in T), whereas cortices isolated mid-late in cytokinesis (S) have a majority of cortices with patchy/filamentous CR patterns (percentages graphed in T). Bar in A = 10 μm and magnifications of A-Q are equivalent. Bar in R = 10 μm and magnification of R and S are equivalent. All cortices from *S. purpuratus* embryos.

https://doi.org/10.1371/journal.pone.0252845.g004

of the myosin II heavy chain (MyoHC) tail and the P-MyoRLC head antibody probes [16] often indicated an extensive overlap of these two regions, suggesting that myosin II filaments may be densely packed (Fig 6A, 6D and 6G). The myosin II stained clusters would often form rings with hollow centers (Figs 6D, 7B and 7C) in which it appeared that myosin II minifilaments were arrayed around the periphery in a head to head circular structure (Fig 7B and 7C). In some stellate-shaped clusters the myosin II minifilaments had adopted the linear alignment of head-to-head chains or networks (Figs 6D, 6G and 7A) that our previous TEM images have shown to exist in the CR in embryos and in the cytoskeleton of coelomocytes [16]. Z axial images indicated a significant superposition between the two myosin II probes, with the suggestion that the myosin II heads might be farther away from the membrane (bottom of image)

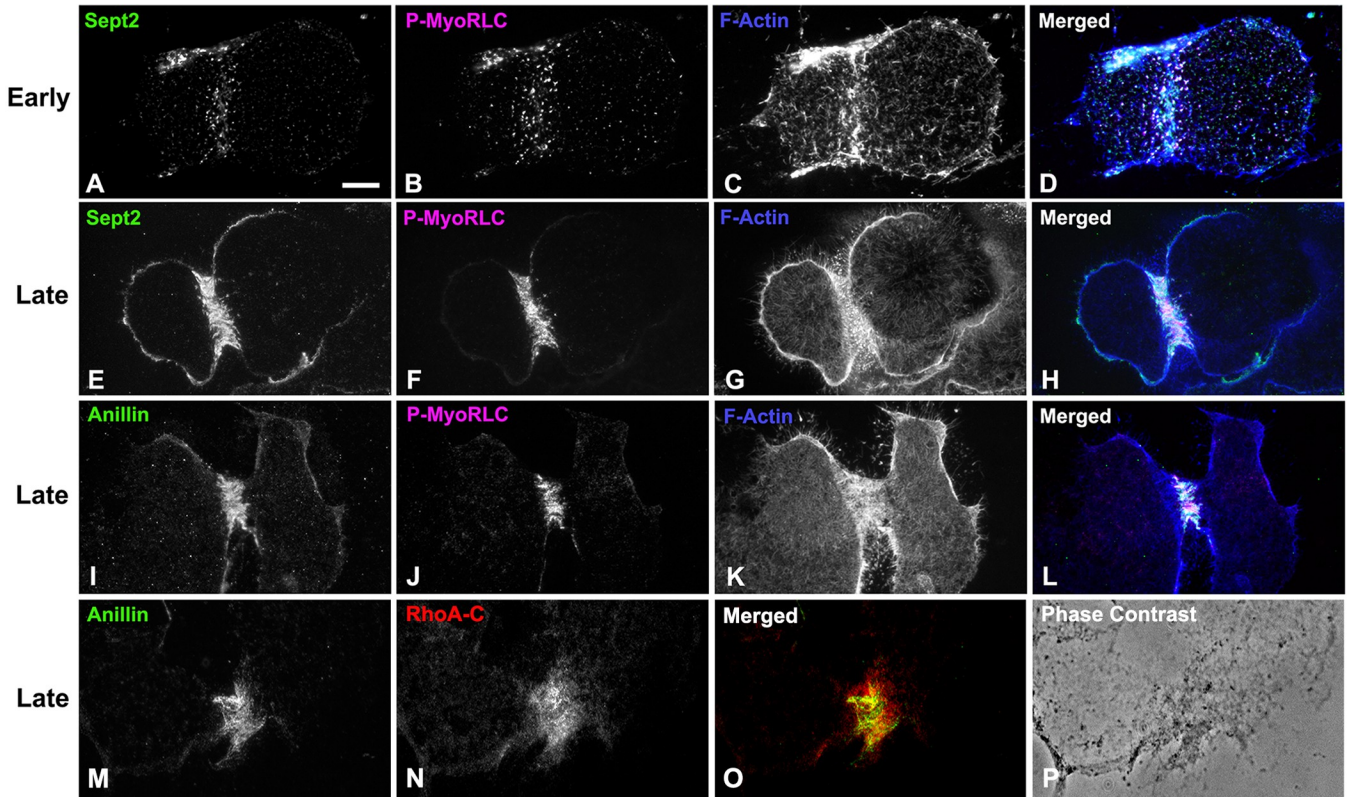

Fig 5. Widefield imaging of isolated cortices demonstrates that septin2 and anillin colocalize with active myosin II, filamentous actin and RhoA/B/C in CRs. Septin2, active myosin II (P-MyoRLC) and F-actin staining all associate with clusters in early CRs (A-D), and with the denser, more linear arrays in late stage CRs (E-H). Anillin displays a similar association with active myosin II and F-actin in late stage CRs (I-L) and also codistributes with Rho A/B/C in the CR (M-P). Bar in A = 10 μm; magnifications of A-L are equivalent. All cortices from *S. purpuratus* embryos.

https://doi.org/10.1371/journal.pone.0252845.g005

than the tail regions (Fig 6J). However, the lower resolution and distorted nature of 3D-SIM Z axial images make it difficult to draw any definitive conclusions.

Imaging of septin2 and P-MyoRLC stained small clusters (diameter < ~1 μm) in cortices with 3D-SIM (Figs 6B, 6E, 6H, 7D and 7E) indicated that septin2 often appeared to be in the center of these clusters relative to the myosin II head staining and this was corroborated by 2D line scans and 3D surface plots of the relative intensity of septin2 and P-MyoRLC staining (Fig 7H and 7I)–with an average of 78% of small clusters containing centralized septin2 (Fig 7L). The pattern of septin2 labeling was often ring-shaped and in some cases resembled short segments of filaments (Fig 6E–6H). The Z axial images of septin2 and P-MyoRLC (Fig 6K) showed overlap and no clear distinction in the orientation of the two labels. 3D-SIM imaging of anillin and P-MyoRLC demonstrated that anillin also appeared to occupy the small cluster centers and was organized in punctate, ring or C-shaped structures that appeared in close proximity to the myosin II head probe (Figs 6C, 6F, 6I, 7F and 7G). 2D line scans and 3D surface plots of the anillin and P-MyoRLC relative intensities (Fig 7J and 7K) corroborated anillin's central location, with 77% of small clusters analyzed showing centralized anillin (Fig 7L). Interestingly, the Z axial images of anillin and P-MyoRLC (Fig 6L) showed a clear distinction in the orientation of the anillin and myosin II head probes with the anillin being closer to the membrane (bottom of image in Fig 6L). For quantification of septin2 and anillin positioning in clusters, 299 total small clusters were analyzed from three separate experiments.

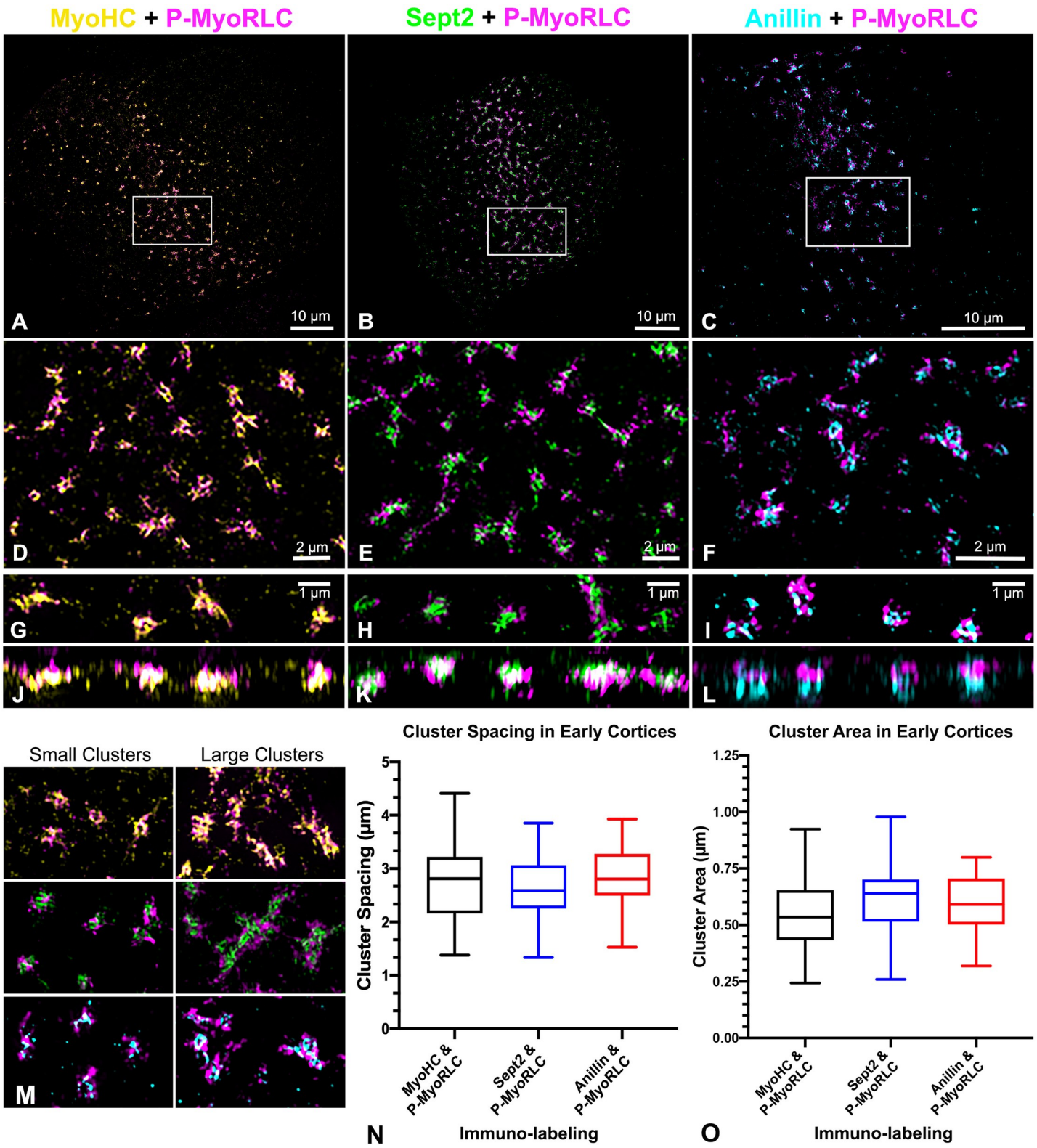

Fig 6. 3D-SIM super-resolution imaging of clusters of myosin II, septin2 and anillin in early CR stage cortices. (A-F) Survey (A-C) and higher magnification views (D-F: enlarged white boxes in A-C) of isolated cortices from dividing embryos double labeled for P-MyoRLC (magenta in A-F) and either MyoHC (yellow in A, D), septin2 (green in B, E), or anillin (cyan in C, F). (G-L) The pairs of images that appear in G&J, H&K and I&L consist of a 10 μm x 3 μm XY image on the top paired with a corresponding 10 μm x 2 μm XZ image of the same clusters on the bottom. (M) In later stage CR regions of isolated cortices clusters become enlarged and appear to

interact/coalesce with one another. Box and whisker plots (min/max with line at median) of small cluster spacing (N) and diameter (O) in early stage cortices stained by the three combinations of antibodies. Bar magnifications as indicated, with images in M equivalent in magnification to panel F. All cortices from *S. purpuratus* embryos.

https://doi.org/10.1371/journal.pone.0252845.g006

Examination of cortices isolated in a time series showed that clusters from cortices later in cytokinesis became larger in size and more extensive (Fig 6M) although they appeared to retain the overall organization of myosin II, septin2, and anillin apparent in smaller clusters. Taken together these images suggest that these myosin II, septin2 and anillin clusters are precursors of the CR and that their growth and coalescence over time generates the mature structure of the CR. They also indicate a codependence in terms of localization given that clusters consistently showed the presence of myosin II and either septin2 or anillin. In terms of physical parameters, the small clusters (diameter < ~1 μm) in early cortices were spaced an average of 2.7 μm apart (Fig 6N) and averaged 0.586 μm in diameter (Fig 6O), with these

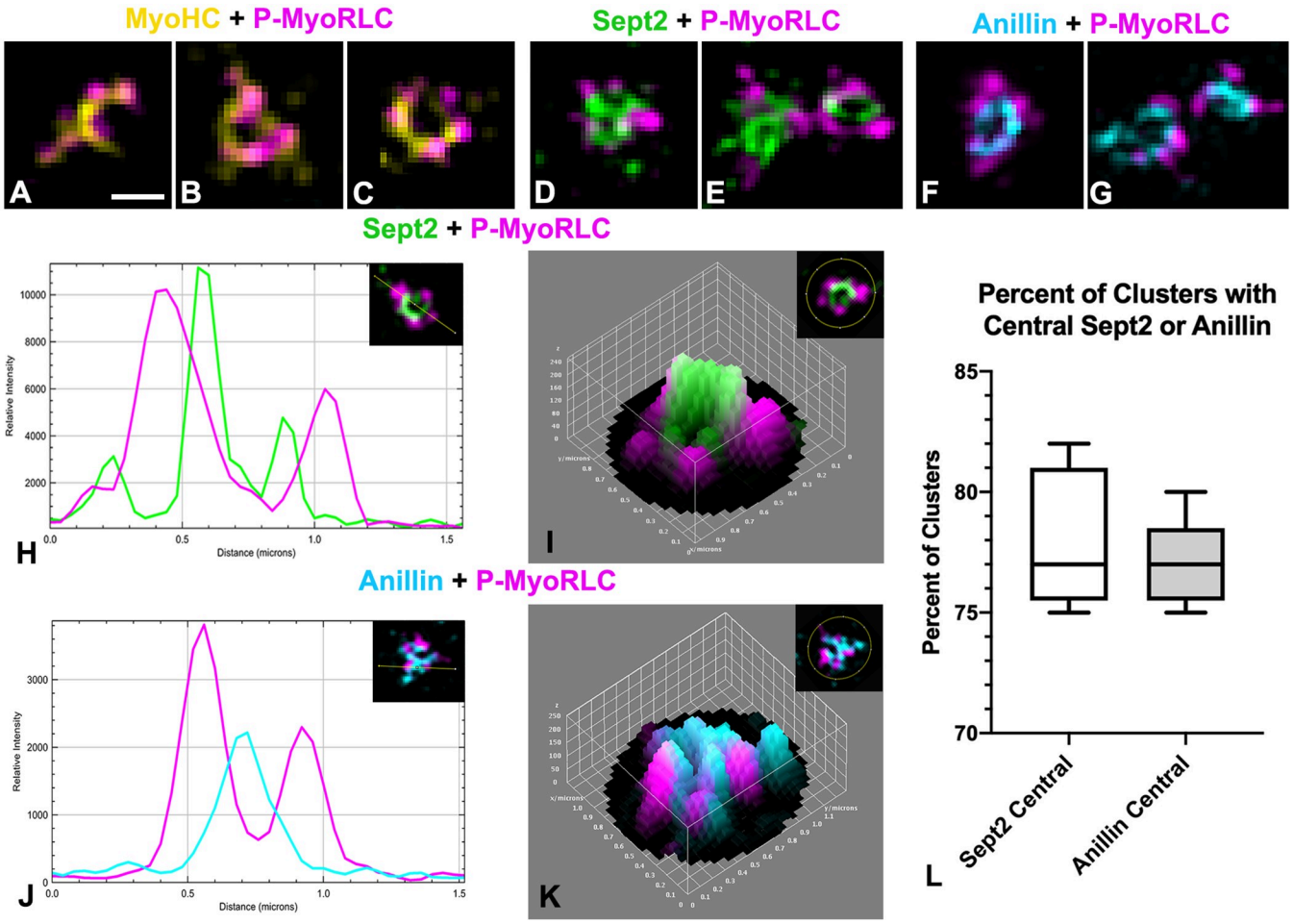

Fig 7. Analysis of early cluster organization using 3D SIM shows that septin2 and anillin tend to be central with myosin II on the periphery. (A-C) MyoHC (yellow) and P-MyoRLC (magenta) staining of early cytokinesis stage small clusters showing what appear to be mini-filaments arranged in chains (A) and rings (B, C). (D-G) Staining of P-MyoRLC (magenta) with either septin2 (green in D, E) or anillin (cyan in F, G) shows peripheral position of myosin II heads and the more central position of septin2 and anillin. (H-K) The central location of septin2 (green in H, I) and anillin (cyan in J, K) was confirmed by analyzing early small clusters with 2D line scans (H, J) and 3D surface plots (I, K) of relative staining intensities. Insets in H-K show images being analyzed and the line or area ROI–the images of clusters in I and K have been rotated to match the orientation of the 3D surface plots. (L) Box and whisker plots (min/max with line at median) of the percent of total early small clusters with centralized septin2 or anillin staining. Bar in A = 500 nm; magnifications of A-G are equivalent. All cortices from *S. purpuratus* embryos.

https://doi.org/10.1371/journal.pone.0252845.g007

measurements not being significantly different in clusters stained with any of the three antibody combinations. This lack of difference is important because it provides assurance that the clusters identified with the three different antibody combinations are the same structures. In terms of comparing the physical parameters of the sea urchin embryo clusters to the nodes that initiate cytokinesis in fission yeast, the sea urchin clusters are larger and more widely spaced as would be expected given the large difference in size between the two cells. In fission yeast nodes are ~500–700 nm apart and average ~100–200 nm in diameter [24,27,63].

Super-resolution microscopy demonstrates the organization of myosin II, anillin and septin2 in the mature CR and suggests evidence of a septin filament network

In isolated cortices containing mature CRs 3D-SIM imaging demonstrated that the pattern of myosin II labeling was linearized with an alignment of chains of head-to-head associated myosin II filaments (Fig 8A–8D), as we have previously reported [16]. In contrast, septin2 staining was organized into a network pattern that was closely associated with P-MyoRLC staining (Fig 8E–8H). The septin2 staining within the network was frequently discontinuous/periodic which may be the result of the septin2 antibody binding to only one of the septin isoforms within the linear structure of a heteropolymer. The overall network pattern of septin2 within the CR appeared similar to the gauze-like organization of septin filaments that has been reported *in vitro* [64,65] and *in vivo* in other cell types [66–68]. One criticism of 3D-SIM microscopy is that the structured illumination itself and/or the associated post-acquisition processing can create a honeycomb pattern artifact in the images [69]. Therefore, in order to corroborate the septin2 network staining seen using 3D-SIM, we imaged cortices using STED microscopy, a higher resolution mode of super-resolution microscopy [70] that does not suffer from this type of artifact. STED images of cortices also showed examples of a septin2 filament network pattern in the CR closely affiliated with myosin II (Figs 8I–8L and 9A–9C). In STED images this network can appear less continuous than in 3D-SIM which may be indicative of the higher resolution showing the separation between septin subunits in the presumably oligo-heteromeric organization of the filaments. Our combined 3D-SIM and STED images provide one of the initial visualizations of an apparent septin filament network structure in the CR of an animal cell.

Imaging of anillin stained mature stage CRs in cortices with 3D-SIM (Fig 8M–8P) showed that unlike septin2, the anillin pattern often appeared less interconnected and more punctate, although it was also closely co-distributed with the myosin II head probe staining in the CR region. In late stage, highly contracted CRs, STED imaging suggested that the anillin pattern appeared to become more network-like (Fig 8Q–8U).

Actin filaments are not required for septin2 or anillin recruitment to early CR clusters

Our previous work [16] and an earlier study from other investigators [20] have shown that treatment of sea urchin embryos with the actin filament disrupting drugs Latrunculin A or B does not disrupt the ability of myosin II to form clusters in the CR region during telophase. Latrunculin treated embryos do not undergo cytokinesis and do not display the linearized pattern of aligned myosin II seen in control embryos [16]. In order to test the actin dependence of septin2 or anillin localization to CR clusters we treated embryos with either LatA or LatB and then fixed and stained embryos and isolated cortices for P-MyoRLC and either septin2 or anillin at time points consistent with the timing of first division telophase in matched control embryos. We also monitored karyokinesis in these Lat treated embryos as this process is not

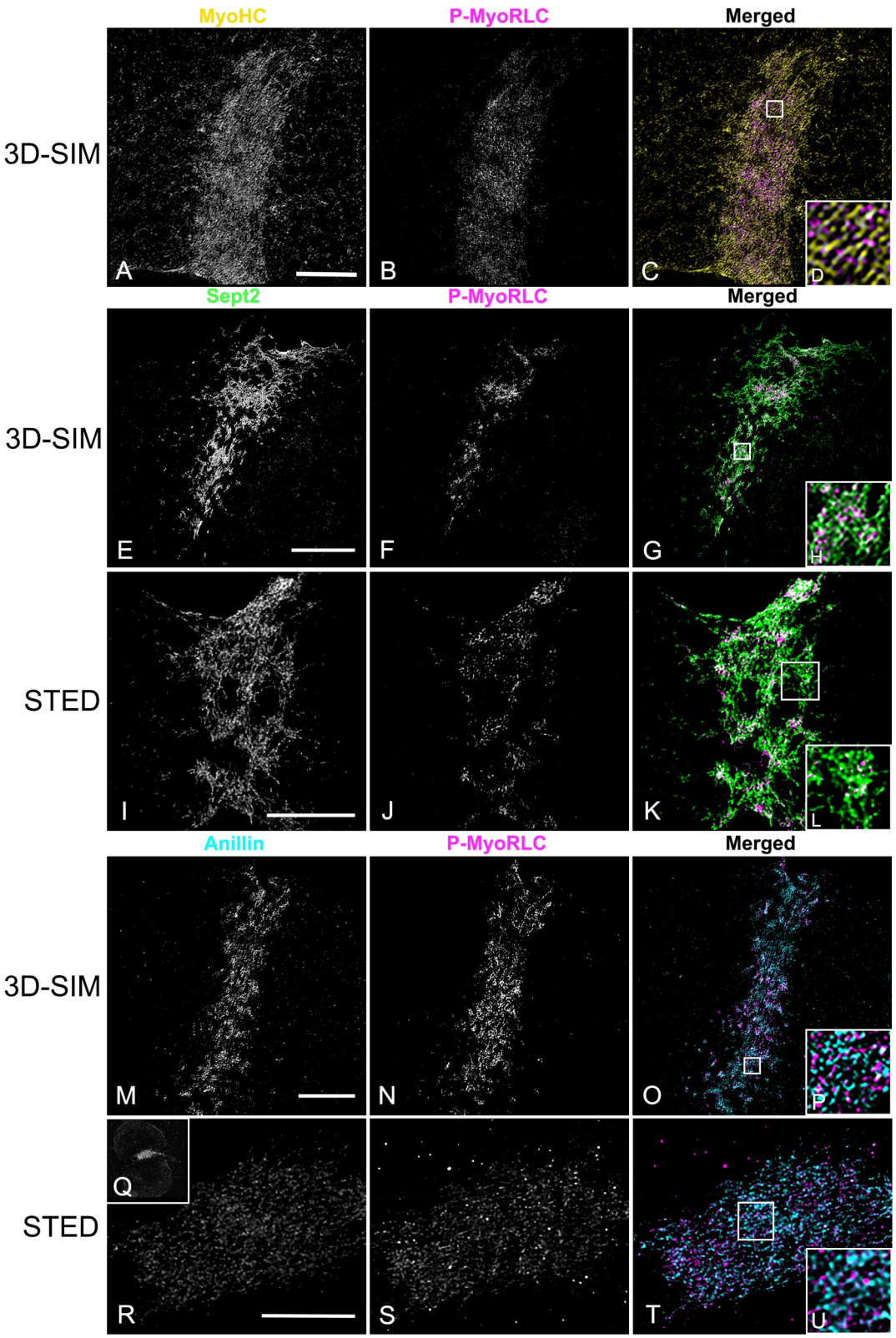

Fig 8. 3D-SIM and STED super-resolution imaging of myosin II, septin2 and anillin in late stage CRs in isolated cortices. (A-D) MyoHC (yellow) and P-MyoRLC (magenta) staining of mature CR showing alignment of head-to-head minifilament chains (C, D). (E-L) Septin2 (green) and P-MyoRLC (magenta) labeling of a late stage CR region showing the network-like

structure of septin2 filaments in close association with myosin II (H, L) using both 3D-SIM (E-H) and STED (I-L) imaging. (M-U) Anillin (cyan) and P-MyoRLC (magenta) staining of a mature CR indicates that anillin is more punctate in distribution and in close proximity to myosin II (M-P). The cortex in Q-V is highly contracted (Q shows a low magnification confocal view) and in this CR remnant the STED imaging of anillin appears similar to a network. White boxes in C, G, K, O, T correspond to the regions that appear at higher magnification in the insets labeled D, H, L, P, U. Bars = 10 μm. All cortices from *S. purpuratus* embryos.

https://doi.org/10.1371/journal.pone.0252845.g008

inhibited by actin filament disruption. In both whole embryos (Fig 10A–10C and 10G–10I) and isolated cortices (Fig 10D–10F and 10J–10L) we saw evidence of an association between P-MyoRLC and septin2 (Fig 10A–10F) or anillin (Fig 10G–10L) in band-like arrays of clusters reminiscent of the early CR (Figs 4–6). Localization of nuclei in whole embryos indicated that they had undergone nuclear division (Fig 10C–10I). Staining of F-actin in control and LatA-treated embryos using fluorescent phalloidin demonstrated that LatA addition resulted in the loss of actin filaments, which inhibited cyto- but not karyo-kinesis (S3 Fig).

Discussion

In a recent cytokinesis review article, Glotzer [2] pointed out that the structural organization of the metazoan animal CR remains poorly understood due to the rapid rearrangements and dense collections of filaments involved which make it difficult to resolve using conventional light microscopy. In our previous study [16] we have addressed these limitations by leveraging the advantage of the sea urchin embryo isolated cortex experimental system combined with super-resolution light microscopy and platinum replica TEM. Our results suggested that the sea urchin embryo CR assembles from an equatorial band of myosin II clusters that coalesce into a linearized arrangement of end-to-end myosin II filaments in the mature CR. In the present study, we confirm and extend our recent work by once again using isolated cortices combined with super-resolution microscopy to explore the nanostructural organization and dynamics of the major CR scaffolding proteins anillin and septin.

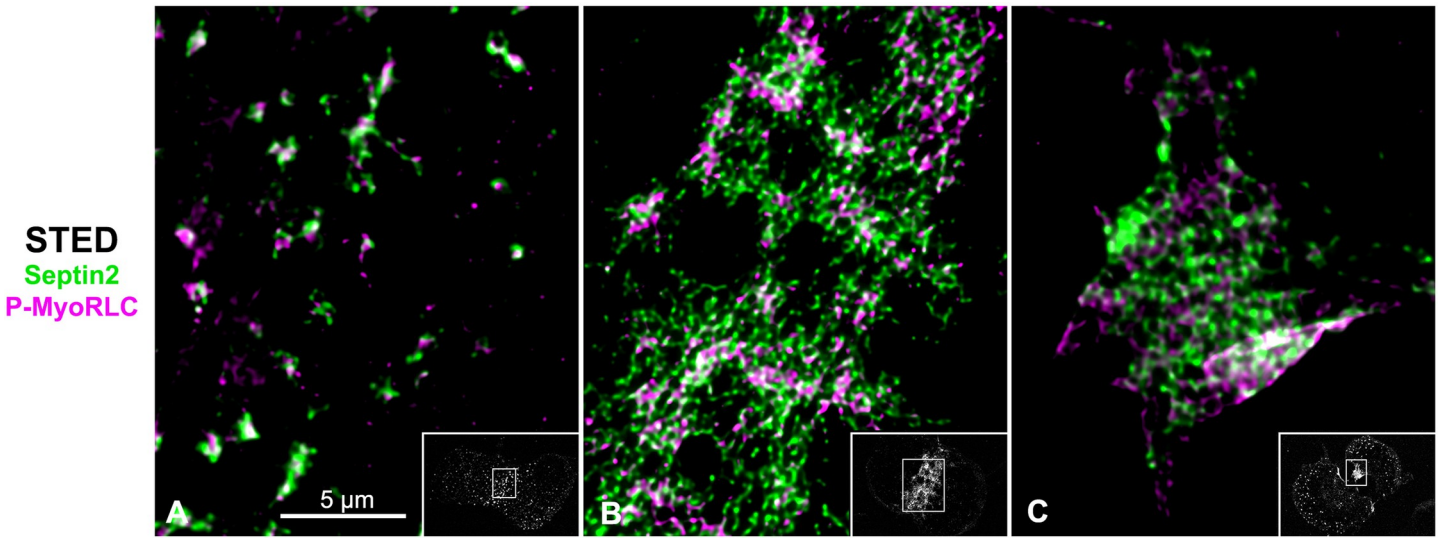

Fig 9. STED imaging of CR septin2 in isolated cortices shows a transformation from clusters to a filamentous network. (A-C) STED imaging of septin2 (green) and P-MyoRLC (magenta) in isolated *S. purpuratus* cortices shows elongate septin2 filaments in enlarging clusters in an early CR (A) versus the filamentous network structure of septin2 staining in later stage CRs (B, C). Insets in A-C show lower magnification confocal images of the cortices with the regions imaged by STED outlined by a white rectangle. Bar = 5 μm; magnifications of A-C are equivalent.

https://doi.org/10.1371/journal.pone.0252845.g009

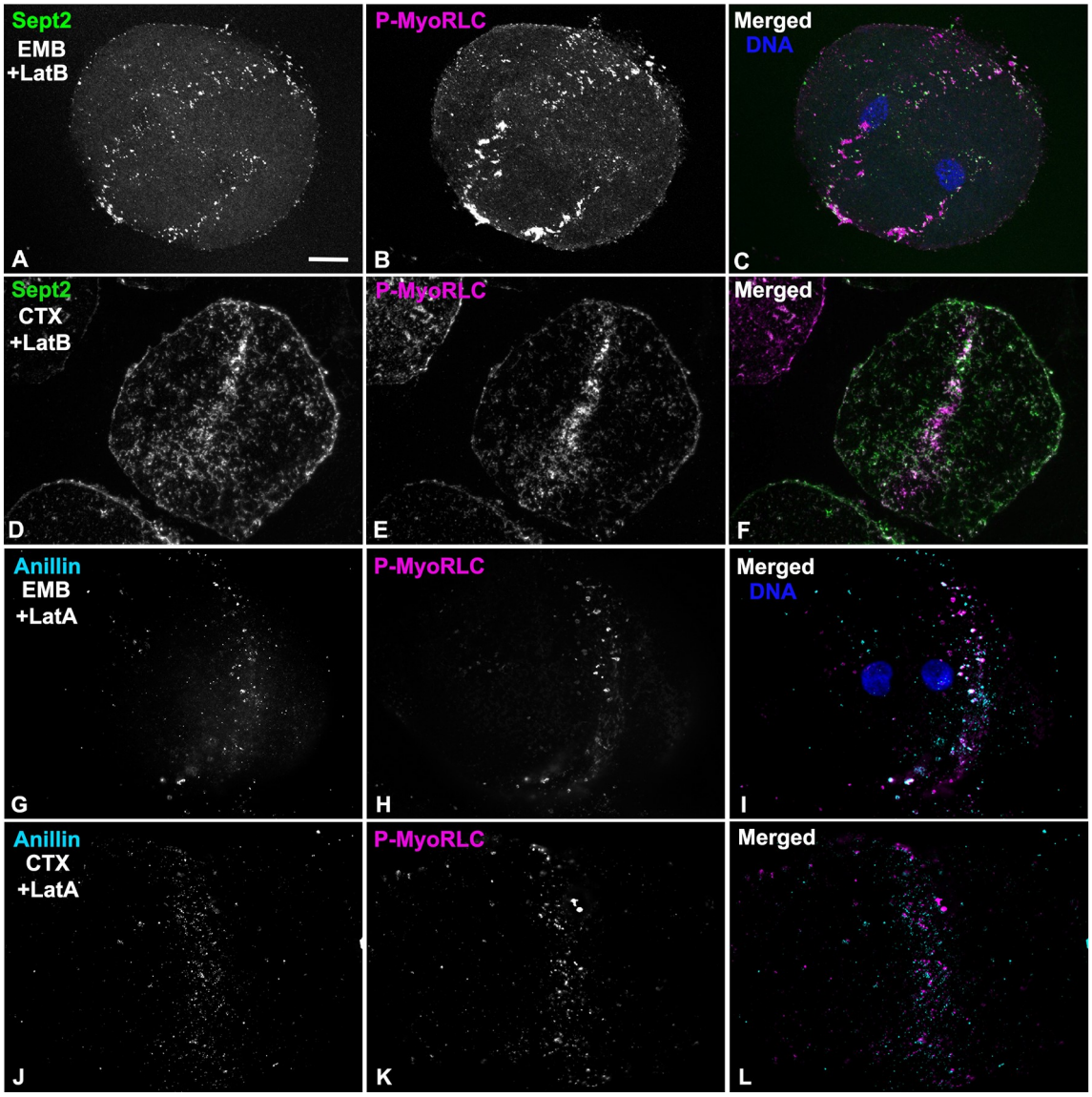

Fig 10. Actin filaments are not required for the recruitment of myosin II, septin2 or anillin to early stage CR clusters. (A-C) Whole embryo (EMB) treated with LatB and stained for septin2 (green), P-MyoRLC (magenta), and DNA (blue) and viewed using a through focus projection of a confocal Z series. The embryo contains a circumferential band of clusters containing myosin II and septin2 and the DNA staining indicates that it has undergone nuclear division during mitosis but not cytokinesis. (D-F) Cortex (CTX) isolated from a LatB treated embryo shows that septin (green) and P-MyoRLC (magenta) localize to a concentrated stripe of clusters. (G-I) Whole embryo (EMB) treated with LatA and stained for anillin (cyan) and P-MyoRLC (magenta) shows they colocalize in a stripe in an embryo which has undergone karyokinesis (I, DNA in blue). (J-L) Cortex (CTX) isolated from a LatA-treated embryo demonstrating a band of anillin and P-MyoRLC clusters. Bar = 10 μm in A; magnifications of A-L are equivalent. *L. pictus* embryos in A-F, *S. purpuratus* embryos in G-L.

https://doi.org/10.1371/journal.pone.0252845.g010

Anillin localization in the sea urchin embryo CR is consistent with its potential scaffold function

Anillin is a CR scaffold protein that localizes to the cleavage furrow where it is essential for cytokinesis and helps integrate RhoA, the membrane, actin, myosin II, formin and septins [36–39,41,71–74]. Despite significant research effort on the structure and function of anillin [42], the precise localization of anillin within the CR is not clear in animal cells, although it is

well-defined in fission yeast. In these cells, the anillin-like protein Mid1 is localized in the nucleus, but upon entry into mitosis, it relocates to an equatorial band, where it forms a number of small nodes [23,24,75]. Mid1 recruits the CR components myosin II (Myo2) and the formin Cdc12 [23,24,27]. Actin filaments nucleated from the nodes via formin activity are then captured by myosin II that in turn pulls the nodes together into a CR-like structure [2,27,63].

In the present study, we investigated anillin localization in the sea urchin embryo CR by an antibody raised against the PH domain of sea urchin anillin (Fig 1), which labeled the cleavage furrow in the expected orientation relative to the mitotic apparatus (Fig 2), and colocalized with the CR marker for activated myosin II (P-MyoRLC, Fig 3). In cortices isolated from first division embryos, conventional imaging revealed that anillin associates with myosin II initially in clusters/nodes that then progress to narrower, more linearized arrays in more mature CRs (Figs 4 and 5). Super-resolution imaging emphasized the close association between anillin and myosin II within the early stage clusters (Figs 6 and 7), with anillin often displaying a C or O-shaped structure in cluster centers, as well as the possibility suggested from Z axial images that anillin resides closer to the membrane relative to myosin II head groups. The fact that anillin localizes to the CR region in clusters independent of actin filaments (Fig 10) is consistent with previous work in *Drosophila* S2 cells [40], but inconsistent with results from BHK-21 mammalian cells [36]. Our overall staining results support the potential CR scaffold function for anillin given that we localize it together with its expected binding partners myosin II, actin, septin, and RhoA (Figs 3–8 and S1).

Our anillin localization results are in general agreement with previous fPALM super-resolution imaging of fission yeast nodes [27] and mature CRs [76] which suggest that the anillin-like Mid1 resides in the center of nodes and nearest the membrane relative to other node/CR proteins. Higher order anillin structures in sea urchin CRs are suggested by 3D-SIM images of late stage CRs where anillin on occasion appears reticular (Fig 8). Earlier work has hinted at organized staining patterns for anillin in the CR, to include the punctate distribution of anillin along actin cables in the cleavage furrow of BHK cells [36], the presence of patches or filaments containing anillin and myosin II in the CR of HeLa cells either untreated or arrested in cytokinesis by blebbistatin treatment [18,38], and the presence of combined anillin and septin rings in the intercellular bridge region of late stage dividing HeLa cells [74].

Septin2 localization in the sea urchin embryo CR demonstrates potential higher order structure

Septins are a family of G proteins first discovered in yeast [77] that can assemble into hetero-oligomeric filaments which consist of different isoforms in different species, and which play important roles in cell polarity, membrane remodeling, morphogenesis, exocytosis, and cytokinesis [7,33]. Septins have long known to be associated with the CR in many different cell types [33] and septin2 in particular has been shown to bind to myosin II and facilitate myosin II activation for cytokinesis [78]. In the present study, we demonstrate that septin2 associates with myosin II, actin and anillin in clusters that appear to serve as the antecedent of the CR (Figs 4–9). Within these clusters septin2 is more central than myosin II (Figs 6 and 7), in the same area as anillin, with XZ imaging suggesting little axial separation between septin2 and myosin II. In fission yeast CR precursor nodes do not contain septin [2], although septin filaments are present in the mature CR [76] and septin filaments form characteristic hourglass and double ring structures in the CR-equivalent structure in budding yeast [32]. Our 3D-SIM and STED images indicate the presence of elongate septin2 filaments associated with enlarging clusters and with the mature CR (Figs 6–9). These septin2 filament-like structures associate with but do not precisely colocalize with myosin II staining and frequently display periodic

labeling, as might be expected if the septin2 antibody is labeling just one septin isoform within a hetero-oligomer. In some images the septin2 staining is elongate (Figs 6, 8 and 9) which may represent the ability of short septin filaments to diffuse in the membrane and anneal into longer filaments via end-to-end associations as has been demonstrated *in vitro* on phospholipid bilayers and *in vivo* in fungi [79]. The ability of septin2 to localize to the CR region independent of actin filaments (Fig 10) is similar to the results reported for the septin Pnut in LatA-treated *Drosophila* S2 cells [40].

The higher order structural organization of septin2 filaments present in mature stage CRs of sea urchin embryos appears to be a reticular network-like organization which is closely associated with the distribution of myosin II (Figs 8 and 9). The imaging does not allow for a distinction between an interconnected network of filaments versus an array of separate filaments in an overlapping organization. However, this septin2 network is reminiscent of the gauze-like septin filament structures that have been previously reported *in vitro* using negative stain TEM [64,65], associated with the cortex of budding yeast *in vivo* using platinum replica TEM [67] and TEM tomography [67], and associated with the interface of transverse and dorsal stress fibers in the leading lamella of migrating mammalian epithelial cells using SIM [68]. Prior work with dividing mammalian tissue culture cells has shown apparent filamentous septin staining codistributed with CR actin cables [36] and septin rings in the midbody at the end of cytokinesis [74].

Clusters of myosin II, anillin and septin initiate the sea urchin embryo CR

Our results suggest that an equatorial band of cortical clusters of myosin II, septin2 and anillin help serve as a precursor for the formation of the CR in first division sea urchin embryos. Earlier work in *C. elegans* embryos [37,39] and in *Drosophila* S2 cultured cells [40] have indicated that clusters of these same three proteins are also involved in the cytokinesis process, although these clusters are not completely analogous to our results and the imaging employed is significantly lower resolution. In *C. elegans* the anillin homologue ANI-1 is required for the cortical ruffling and pseudocleavage that proceed cytokinesis as well as for asymmetric cleavage patterns during cytokinesis, although CR closure can occur in the absence of ANI-1 [37,39]. In addition, ANI-1 targets independently to the CR and helps direct septins, but not myosin II, there as well. In contrast with the equatorial band of clusters we demonstrate in the sea urchin embryo, the clusters in *C. elegans* appear distributed throughout the entire cortex of the embryo during ruffling, although clusters of myosin II do appear in the CR region during cytokinesis [22]. In S2 cells the CR localization of anillin is independent of actin and myosin II, its absence causes destabilization of the position of the cleavage furrow, and aggregates of myosin II, anillin and septin in the CR only become obvious upon treatment of dividing cells with Latrunculin [40]. These aggregates can appear filamentous with myosin II and anillin staining appearing in the same place but slightly offset [40], reminiscent of what we demonstrate in our SIM images of anillin and myosin II staining of clusters. In general, it appears that the cytokinetic myosin II, anillin and septin clusters in *C. elegans* embryos and in *Drosophila* S2 cells are loosely analogous with those we demonstrate in the sea urchin embryo. However, the differences outlined above, the superior spatial resolution of the architecture of clusters we provide, as well as the strong evidence of the transformation of the sea urchin clusters into patches and linearized arrays makes it difficult to make more direct comparisons.

A working conceptual model for how the CR is built in the early sea urchin embryo

Our current conceptual model of CR formation in the first division sea urchin embryo employs the following hypothetical framework as informed by the results of our present study.

At late anaphase the astral microtubule-dependent activation of Rho via the action of centralspindlin/RhoGEF helps trigger the recruitment of anillin, myosin II and septin to the CR precursor clusters (Figs 4–7), which is facilitated by the ability of these three CR components to bind to one another. Within the clusters anillin and septin occupy a central core (Figs 6 and 7) and would be expected to interact with the membrane and bind with the tails of myosin II filaments. Actin filaments are not necessary for the recruitment of myosin II [16,20], septin (Fig 10), or anillin (Fig 10) to the CR region in sea urchin embryos and research in other cell types suggests that anillin recruitment is independent of myosin II, whereas septin recruitment is dependent on anillin [37,39,40]. As noted earlier, the sea urchin clusters share some gross similarities with the organization of clusters of these proteins in dividing *C. elegans* embryos and *Drosophila* S2 cells as well as the nodes seen in fission yeast undergoing cytokinesis. However, the yeast nodes do not contain septin and the orientation of the myosin II filaments in our images suggests a mini-filament chain organization instead of the bouquets of individual myosin II proteins defined by fPALM imaging of yeast nodes [27]. Over time the sea urchin clusters enlarge with myosin II forming head-to-head filament arrays oriented parallel to the plane of the membrane via interaction with actin filaments, septin filaments elongating via annealing with other septin oligomers [79], and the anillin array also expanding (Figs 6 and 7). In fission yeast nodes anillin/Mid1 activates formins that nucleate actin filaments which then are used by node-associated myosin II to move the nodes towards the forming CR [28,63]. Actin filaments do associate with the sea urchin clusters (Fig 5), however the distribution of formin has not been established in our system. Coincident with cluster enlargement these structures tend to interconnect and coalesce into a narrower and denser linear array in which the interaction of myosin II with elongate actin filaments causes them to become aligned parallel with the axis of the cleavage furrow (Figs 5 and 8), septin filaments organize into a network (Figs 8 and 9), whereas anillin tends to remain in more punctate arrays until late in cleavage where they also appear to form a network (Fig 8).

Within the context of the mature CR, septin and anillin can be considered to be functioning as scaffold and anchoring proteins although they also may engage in other critical roles. For example, septins may be contributing to the full activation of myosin II by serving as a platform for myosin II and its activating kinases [78], and/or they may be essential for the curvature and bundling of the actin filaments in the CR [33,80]. In the sea urchin embryo septin and anillin remain in the CR through the midbody stage (Figs 2 and 3) and therefore may be expected to play a role in the maturation of the CR to the midbody and subsequent abscission given the evidence that they participate in this critical step in other cells [74,81–84].

In conclusion, the results of the present study suggest that CR generation in sea urchin embryos may be an evolutionary derivative of the process in fission yeast, with both mechanisms relying on initiation via clusters/nodes of crucial cytokinetic proteins, including myosin II, anillin, actin, and, in the sea urchin, septin. In order to further explore this evolutionary relationship and to address the many questions raised by our hypothetical conceptual model, we are currently pursuing a number of new experimental directions. These include CR imaging approaches in live embryos to more closely examine dynamics, investigations into the role of formins in CR formation, and development of agent-based computer modeling of cytokinesis informed by our microscopy-based studies.

Supporting information

S1 Fig. Anillin persists at the midbody following cytokinesis. Anillin (A, E, and I—green), P-MyoRLC (B, F, and J—red), and microtubules (C, G, and K—cyan) were imaged in *S. purpuratus* embryos at the end of cytokinesis by confocal microscopy. In the late ingressing

embryos (A-H), anillin and P-MyoRLC are enriched in the contractile ring (A-D), as well as the forming midbody (E-H). Anillin remains associated with the midbody after the contractile ring has completed constriction and P-MyoRLC staining is lost (I-L). Bar, 15 μm.
(TIF)

S2 Fig. Widefield imaging of directly labeled septin2 and anillin antibody staining in isolated first division cortices. Sept2 (A, E, C, and G—green) and anillin (B, F, C, and G—blue) antibodies labeled with the Zenon rabbit IgG labeling kit (Molecular Probes) show a general colocalization within the CR region of double labeled mid-late stage isolated cortices from *S. purpuratus*. Bar in A = 10 μm, magnifications of A-H are equivalent.
(TIF)

S3 Fig. LatA treatment depolymerizes actin filaments and inhibits cytokinesis. Staining of control (A-D) and LatA treated (E-H) whole *S. purpuratus* embryos with fluorescent phalloidin (green) and DAPI (blue) at equivalent time points shows LatA-mediated loss of actin filaments and inhibition of cytokinesis–but not karyokinesis. The control embryo in panel B shows F-actin in the clusters stage of CR organization, whereas the later stage control embryo in panel D shows a clear linearized ring. The cortical microvilli-associated phalloidin staining present in control embryos is not seen in the LatA treated embryos. Bar in A = 10 μm, magnifications of A-H are equivalent, and all images are widefield.
(TIF)

S1 File. Original immunoblots from Fig 1B and 1C. Panel A is the full anti-anillin immunoblot from Fig 1B. Lane 1 = PH domain immunogen; Lane 2 = *S. purpuratus* egg; Lane 3 = *S. purpuratus* first division embryo. Panel B corresponds to the total protein Poncea S stained anti-Sept2 blot from Fig 1C. Panel C corresponds to Fig 1C anti-Sept2 immunoblot of the original blot destained for total protein. In panels B and C: Lane 1 = *L. pictus* first division embryo; Lane 2 = LLC-PK1 cells; Lane 3 = Prestained molecular weight standards.
(PDF)

S1 Spreadsheet. Data sets used for graphs in Figs 4T, 6N, 6O and 7L.
(XLSX)

Acknowledgments

Grateful thanks are extended to Dr. Simon Watkins and Michael Calderon (Center for Biologic Imaging, University of Pittsburg) for their expert assistance with STED microscopy, to Dr. Billie Swalla (University of Washington) for access to instrumentation and reagents at Friday Harbor Laboratories (FHL), and to Casey Ditzler, Aphnie Germain, Patrick Irwin, Eric Vogt, Erik Williams, Bakary Samasa, Ethan Burg, and Hannah Herzon (Dickinson College) for help with experimentation and image analysis.

Author Contributions

Conceptualization: Chelsea Garno, Charles B. Shuster, John H. Henson.

Data curation: Chelsea Garno, Zoe H. Irons, Courtney M. Gamache, Charles B. Shuster, John H. Henson.

Formal analysis: Chelsea Garno, Zoe H. Irons, Courtney M. Gamache, Charles B. Shuster, John H. Henson.

Funding acquisition: Charles B. Shuster, John H. Henson.

Investigation: Chelsea Garno, Zoe H. Irons, Courtney M. Gamache, Quenelle McKim, Gabriela Reyes, Xufeng Wu, Charles B. Shuster, John H. Henson.

Methodology: Chelsea Garno, Zoe H. Irons, Courtney M. Gamache, Xufeng Wu, Charles B. Shuster, John H. Henson.

Project administration: Charles B. Shuster, John H. Henson.

Resources: Xufeng Wu.

Supervision: Charles B. Shuster, John H. Henson.

Validation: Chelsea Garno, Charles B. Shuster.

Visualization: Quenelle McKim, Gabriela Reyes, Charles B. Shuster, John H. Henson.

Writing – original draft: Chelsea Garno, John H. Henson.

Writing – review & editing: Chelsea Garno, Charles B. Shuster, John H. Henson.

References

1. Pollard T. D. (2017). Nine unanswered questions about cytokinesis. *Journal of Cell Biology*, 216, 3007–3016. https://doi.org/10.1083/jcb.201612068 PMID: 28807993
2. Glotzer M. (2017). Cytokinesis in metazoa and fungi. *Cold Spring Harbor Perspectives in Biology*, 9 (10):a022343. https://doi.org/10.1101/cshperspect.a022343 PMID: 28007751
3. Mangione M. C., & Gould K. L. (2019). Molecular form and function of the cytokinetic ring. *Journal of Cell Science*, 132, jcs226928. https://doi.org/10.1242/jcs.226928 PMID: 31209062
4. Pollard T. D., & O'Shaughnessy B. (2019). Molecular mechanism of cytokinesis. *Annual Review of Biochemistry*, 88, 661–689. https://doi.org/10.1146/annurev-biochem-062917-012530 PMID: 30649923
5. Willet A. H., McDonald N. A., & Gould K. L. (2015). Regulation of contractile ring formation and septation in *Schizosaccharomyces pombe*. *Current Opinion in Microbiology*, 28, 46–52. https://doi.org/10.1016/j.mib.2015.08.001 PMID: 26340438
6. Meitinger F., & Palani S. (2016). Actomyosin ring driven cytokinesis in budding yeast. *Seminars in Cell and Developmental Biology*, 53,19–27. https://doi.org/10.1016/j.semcdb.2016.01.043 PMID: 26845196
7. Marquardt J., Chen X., & Bi E. (2019). Architecture, remodeling, and functions of the septin cytoskeleton. *Cytoskeleton*, 76, 7–14. https://doi.org/10.1002/cm.21475 PMID: 29979831
8. Schroeder T. E. (1970). The contractile ring. I. Fine structure of dividing mammalian (HeLa) cells and the effects of cytochalasin B. *Zeitschrift für Zellforschung und Mikroskopische* Anatomie, 109, 431–449. PMID: 5498229
9. Schroeder T. E. (1972) The contractile ring. II. Determining its brief existence, volumetric changes, and vital role in cleaving *Arbacia* eggs. *Journal of Cell Biology*, 53, 419–434. http://doi.org/10.1083/jcb.53.2.419.
10. Schroeder T. E. (1973). Actin in dividing cells: contractile ring filaments bind heavy meromyosin. *Proceedings of the National Academy of Sciences USA*, 70, 1688–1692. https://doi.org/10.1073/pnas.70.6.1688 PMID: 4578441
11. Perry M. M., John H. A., & Thomas N. S. (1971). Actin-like filaments in the cleavage furrow of newt egg. *Experimental Cell Research*, 65, 249–253. https://doi.org/10.1016/s0014-4827(71)80075-7 PMID: 4101164
12. Sanger J. M., & Sanger J. W. (1980). Banding and polarity of actin filaments in interphase and cleaving cells. *Journal of Cell Biology*, 86, 568–575. https://doi.org/10.1083/jcb.86.2.568 PMID: 6995468
13. Maupin P., & Pollard T. D. (1986). Arrangement of actin filaments and myosin-like filaments in the contractile ring and of actin-like filaments in the mitotic spindle of dividing HeLa cells. *Journal of Ultrastructure and Molecular Structure Research*, 94, 92–103. https://doi.org/10.1016/0889-1605(86)90055-8 PMID: 3772181
14. Beach J. R., Shao L., Remmert K., Li D., Betzig E., & Hammer J. A. (2014). Nonmuscle myosin II isoforms coassemble in living cells. *Current Biology*, 24, 1160–1166. https://doi.org/10.1016/j.cub.2014.03.071 PMID: 24814144

15. Fenix A. M., Taneja N., Buttler C. A., Lewis J., Van Engelenburg S. B., Ohi R., & Burnette D. T. (2016). Expansion and concatenation of non-muscle myosin IIA filaments drive cellular contractile system formation during interphase and mitosis. *Molecular Biology of the Cell*, 27, 1465–1478. https://doi.org/10.1091/mbc.E15-10-0725 PMID: 26960797

16. Henson J. H., Ditzler C. E., Germain A., Irwin P. M., Vogt E. T., Yang S., Wu X., & Shuster C. B. (2017). The ultrastructural organization of actin and myosin II filaments in the contractile ring: new support for an old model of cytokinesis. *Molecular Biology of the Cell*, 28, 613–623. https://doi.org/10.1091/mbc.E16-06-0466 PMID: 28057763

17. Maupin P., Phillips C. L., Adelstein R. S., & Pollard T. D. (1994). Differential localization of myosin-II isozymes in human cultured cells and blood cells. *Journal of Cell Science*, 107, 3077–3090. PMID: 7699007

18. Straight A. F., Cheung A., Limouze J., Chen I., Westwood N. J., Sellers J. R., Field C. M., & Mitchison T. J. (2003). Dissecting temporal and spatial control of cytokinesis with a myosin II inhibitor. *Science*, 299, 1743–1747. https://doi.org/10.1126/science.1081412 PMID: 12637748

19. Werner M., Munro E., & Glotzer M. (2007). Astral signals spatially bias cortical myosin recruitment to break symmetry and promote cytokinesis. *Current Biology*, 17, 1286–1297. https://doi.org/10.1016/j.cub.2007.06.070 PMID: 17669650

20. Foe V. E., & von Dassow G. (2008). Stable and dynamic microtubules coordinately shape the myosin activation zone during cytokinetic furrow formation. *Journal Cell Biology*, 183, 457–470. https://doi.org/10.1083/jcb.200807128 PMID: 18955555

21. Zhou M., & Wang Y. L. (2008). Distinct pathways for the early recruitment of myosin II and actin to the cytokinetic furrow. *Molecular Biology of the Cell*, 19, 318–326. https://doi.org/10.1091/mbc.e07-08-0783 PMID: 17959823

22. Osório D. S., Chan F-Y., Saramago J., Leite J., Silva A. M., Sobral, Gassmann R., & Carvalho A. X. (2019). Crosslinking activity of non-muscle myosin II is not sufficient for embryonic cytokinesis in *C. elegans*. *Development*, 146, dev179150. https://doi.org/10.1242/dev.179150 PMID: 31582415

23. Wu J. Q., Kuhn J. R., Kovar D. R., & Pollard T. D. (2003). Spatial and temporal pathway for assembly and constriction of the contractile ring in fission yeast cytokinesis. *Developmental Cell*, 5, 723–734. https://doi.org/10.1016/s1534-5807(03)00324-1 PMID: 14602073

24. Wu J. Q., Sirotkin V., Kovar D. R., Lord M., Beltzner C. C., Kuhn J. R., & Pollard T. D. (2006). Assembly of the cytokinetic contractile ring from a broad band of nodes in fission yeast. *Journal of Cell Biology*, 174, 391–402. https://doi.org/10.1083/jcb.200602032 PMID: 16864655

25. Pollard T. D., & Wu J. Q. (2010). Understanding cytokinesis: lessons from fission yeast. *Nature Reviews Molecular Cell Biology*, 11, 149–155. https://doi.org/10.1038/nrm2834 PMID: 20094054

26. Lee I-J., Coffman V. C., & Wu J-Q. (2012). Contractile-ring assembly in fission yeast cytokinesis: recent advances and new perspectives. *Cytoskeleton*, 69, 751–763. https://doi.org/10.1002/cm.21052 PMID: 22887981

27. Laplante C., Huang F., Tebbs I. R., Bewersdorf J., & Pollard T. D. (2016). Molecular organization of cytokinesis nodes and contractile rings by super-resolution fluorescence microscopy of live fission yeast. *Proceedings of the National Academy of Sciences USA*, 113, E5876–E5885. https://doi.org/10.1073/pnas.1608252113 PMID: 27647921

28. Vavylonis D., Wu J. Q., Hao S., O'Shaughnessy B., & Pollard T. D. (2008). Assembly mechanism of the contractile ring for cytokinesis by fission yeast. *Science*, 319, 97–100. https://doi.org/10.1126/science.1151086 PMID: 18079366

29. Cheffings T. H., Burroughs N. J., & Balasubramanian M. K. (2016). Actomyosin ring formation and tension generation in eukaryotic cytokinesis. *Current Biology*, 26, R19–R37. https://doi.org/10.1016/j.cub.2016.06.071 PMID: 27505246

30. Lord M., Laves E., & Pollard T. D. (2005). Cytokinesis depends on the motor domains of myosin-II in fission yeast but not in budding yeast. *Molecular Biology of the Cell*, 16, 5346–5355. https://doi.org/10.1091/mbc.e05-07-0601 PMID: 16148042

31. Ma X., Kovács M., Conti M. A., Wang A., Zhang Y., Sellers J. R., & Adelstein R. S. (2012). Nonmuscle myosin II exerts tension but does not translocate actin in vertebrate cytokinesis. *Proceedings of the National Academy of Sciences USA*, 109, 4509–4514 https://doi.org/10.1073/pnas.1116268109.

32. Ong K., Wloka C., Okada S., Svitkina T., & Bi E. (2014). Architecture and dynamic remodelling of the septin cytoskeleton during the cell cycle. *Nature Communications*, 5, 5698. https://doi.org/10.1038/ncomms6698 PMID: 25474997

33. Bridges A. A., & Gladfelter A. S. (2015). Septin form and function at the cell cortex. *Journal of Biological Chemistry*, 290, 17173–17180. https://doi.org/10.1074/jbc.R114.634444.

34. Spiliotis E. T. (2018). Spatial effects—site-specific regulation of actin and microtubule organization by septin GTPases. *Journal of Cell Science* 131. https://doi.org/10.1242/jcs.207555 PMID: 29326311

35. Field C. M., & Alberts B. M. (1995). Anillin, a contractile ring protein that cycles from the nucleus to the cell cortex. *Journal of Cell Biology*, 131, 165–178. https://doi.org/10.1083/jcb.131.1.165 PMID: 7559773

36. Oegema K., Savoian M. S., Mitchison T. J., & Field C. M. (2000). Functional analysis of a human homologue of the *Drosophila* actin binding protein anillin suggests a role in cytokinesis. *Journal Cell Biology*, 150, 539–552. https://doi.org/10.1083/jcb.150.3.539 PMID: 10931866

37. Maddox A. S., Habermann B., Desai A., & Oegema K. (2005). Distinct roles for two *C. elegans* anillins in the gonad and early embryo. *Development*, 132, 2837–2848. https://doi.org/10.1242/dev.01828 PMID: 15930113

38. Straight A. F., Field C. M., & Mitchison T. J. (2005). Anillin binds nonmuscle myosin II and regulates the contractile ring. *Molecular Biology of the Cell* 16, 193–201. https://doi.org/10.1091/mbc.e04-08-0758 PMID: 15496454

39. Maddox A. S., Lewellyn L., Desai A., & Oegema K. (2007). Anillin and the septins promote asymmetric ingression of the cytokinetic furrow. *Developmental Cell*, 12, 827–835. https://doi.org/10.1016/j.devcel.2007.02.018 PMID: 17488632

40. Hickson G. R., & O'Farrell P. H. (2008). Rho-dependent control of anillin behavior during cytokinesis. *Journal of Cell* Biology, 180, 285–294. https://doi.org/10.1083/jcb.200709005 PMID: 18209105

41. Piekny A. J., & Glotzer M. (2008). Anillin is a scaffold protein that links RhoA, actin, and myosin during cytokinesis. *Current Biology*, 18, 30–36. https://doi.org/10.1016/j.cub.2007.11.068 PMID: 18158243

42. Piekny A. J., & Maddox A. S. (2010). The myriad roles of Anillin during cytokinesis. *Seminars in Cell and Developmental Biology*, 21, 881–891. https://doi.org/10.1016/j.semcdb.2010.08.002 PMID: 20732437

43. Mabuchi I., & Okuno M. (1977). The effect of myosin antibody on the division of starfish blastomeres. *Journal of Cell Biology*, 74, 251–263. https://doi.org/10.1083/jcb.74.1.251 PMID: 141455

44. Mabuchi I., Hamaguchi Y., Fujimoto H., Morii N., Mishima M., & Narumiya S. (1993). A Rho-like protein is involved in the organisation of the contractile ring in dividing sand dollar eggs. *Zygote*, 1, 325–331. https://doi.org/10.1017/s0967199400001659 PMID: 8081830

45. Bement W. M., Benink H. A., & von Dassow G. (2005). A microtubule-dependent zone of active RhoA during cleavage plane specification. *Journal of Cell Biology*, 170, 91–101. https://doi.org/10.1083/jcb.200501131 PMID: 15998801

46. Henson J. H., Samasa B., & Burg E. C. (2019). High resolution imaging of the cortex isolated from sea urchin eggs and embryos. *Methods in Cell Biology*, 151, 419–432. https://doi.org/10.1016/bs.mcb.2019.01.005 PMID: 30948022

47. Yonemura S., & Kinoshita S. (1986). Actin filament organization in the sand dollar egg cortex. *Developmental Biology*, 115, 171–183. https://doi.org/10.1016/0012-1606(86)90238-1.

48. Otto J. J., & Schroeder T. E. (1990). Association of actin and myosin in the contractile ring. *Annals of the New York Academy of Sciences*, 582, 179–184. https://doi.org/10.1111/j.1749-6632.1990.tb21678.x PMID: 2192594

49. Mabuchi I. (1994). Cleavage furrow: timing of emergence of contractile ring actin filaments and establishment of the contractile ring by filament bundling in sea urchin eggs. *Journal of Cell Science* 107, 1853–1862. PMID: 7983152

50. Uehara R., Hosoya H., & Mabuchi I. (2008). In vivo phosphorylation of regulatory light chain of myosin II in sea urchin eggs and its role in controlling myosin localization and function during cytokinesis. *Cell Motility and the Cytoskeleton*, 65, 100–115. https://doi.org/10.1002/cm.20246 PMID: 17968985

51. Henson J. H., Svitkina T. M., Burns A. R., Hughes H. E., MacPartland K. J., Nazarian R., & Borisy G. G. (1999). Two components of actin-based retrograde flow in sea urchin coelomocytes. *Molecular Biology of the Cell*, 10, 4075–4090. https://doi.org/10.1091/mbc.10.12.4075 PMID: 10588644

52. Smith L. C., Hawley T. S., Henson J. H., Majeske A. J., Oren M., & Rosental B. (2019). Methods for collection, handling and analysis of sea urchin coelomocytes. *Methods in Cell Biology*, 150, 357–38. https://doi.org/10.1016/bs.mcb.2018.11.009 PMID: 30777184

53. Yonemura S., Hirao-Minakuchi K., & Nishimura Y. (2004). Rho localization in cells and tissues. *Experimental Cell Research*, 295, 300–314. https://doi.org/10.1016/j.yexcr.2004.01.005 PMID: 15093731

54. Gustafsson M. G., Shao L., Carlton P. M., Wang C. J., Golubovskaya I. N., Cande W. Z., Agard D. A., & Sedat J. W. (2008). Three-dimensional resolution doubling in wide-field fluorescence microscopy by structured illumination. *Biophysics Journal*, 94, 4957–497. https://doi.org/10.1529/biophysj.107.120345 PMID: 18326650

55. Hell S. W., & Wichmann J. (1994). Breaking the diffraction resolution limit by stimulated emission: Stimulated-emission-depletion fluorescence microscopy. *Optics Letters* 19, 780–782. https://doi.org/10.1364/ol.19.000780 PMID: 19844443

56. Cao L., Ding X., Yu W., Yang X., Shen S., & Yu L. (2007). Phylogenetic and evolutionary analysis of the septin protein family in metazoan. *FEBS Letters*, 581, 5526–5532. https://doi.org/10.1016/j.febslet.2007.10.032 PMID: 17967425

57. Chen A., Akhshi T. K., Lavoie B. D., & Wilde A. (2015). Importin ß2 mediates the spatio-temporal regulation of anillin through a noncanonical nuclear localization signal nuclear targeting of anillin. *Journal of Biological Chemistry*, 290, 13500–13509. https://doi.org/10.1074/jbc.M115.649160.

58. Beaudet C., Akhshi T., Phillipp J., Law C., & Piekny A. (2017). Active Ran regulates anillin function during cytokinesis. *Molecular Biology of the Cell*, 28, 3517–3531. https://doi.org/10.1091/mbc.E17-04-0253 PMID: 28931593

59. Palander O., El-Zeiry M., & Trimble W. S. (2017). Uncovering the roles of septins in cilia. *Fronteirs in Cell and Developmental Biol*ogy, 5, 36. https://doi.org/10.3389/fcell.2017.00036 PMID: 28428954

60. Argiros H., Henson L., Holguin C., Foe V., & Shuster C. B. (2012). Centralspindlin and chromosomal passenger complex behavior during normal and Rappaport furrow specification in echinoderm embryos. *Cytoskeleton*, 69, 840–853. https://doi.org/10.1002/cm.21061 PMID: 22887753

61. Su K-C., Bement W. M., Petronczki M., & von Dassow G. (2014). An astral simulacrum of the central spindle accounts for normal, spindle-less, and anucleate cytokinesis in echinoderm embryos. *Molecular Biology of the Cell*, 25, 4049–4062. https://doi.org/10.1091/mbc.E14-04-0859 PMID: 25298401

62. Kim H., Johnson J. M., Lera R. F., Brahma S., & Burkard M. E. (2017). Anillin phosphorylation controls timely membrane association and successful cytokinesis. *PLoS Genetics*, 13(1), e1006511. https://doi.org/10.1371/journal.pgen.1006511 PMID: 28081137

63. Laporte D., Coffman V. C., Lee I-J., & Wu J-Q. (2011). Assembly and architecture of precursor nodes during fission yeast cytokinesis. *Journal of Cell Biology*, 192, 1005–1021. https://doi.org/10.1083/jcb.201008171 PMID: 21422229

64. Bertin A., McMurray M. A., Thai L., Garcia G. 3rd, Votin V., Grob P., Allyn T., Thorner J., & Nogales E. (2010). Phosphatidylinositol-4,5- bisphosphate promotes budding yeast septin filament assembly and organization. *Journal of Molecular Biology*, 404, 711–731. https://doi.org/10.1016/j.jmb.2010.10.002 PMID: 20951708

65. Garcia G. III, Bertin A., Li Z., Song Y., McMurray M., Thorner J., & Nogales E. (2011). Subunit-dependent modulation of septin assembly: budding yeast septin Shs1 promotes ring and gauze formation. *Journal Cell Biology*, 195, 993–1004. https://doi.org/10.1083/jcb.201107123.

66. Rodal A. A., Kozubowski L., Goode B. L., Drubin D. G., & Hartwig J. H. (2005). Actin and septin ultrastructures at the budding yeast cell cortex. *Molecular Biology of the Cell*, 16, 372–384. https://doi.org/10.1091/mbc.e04-08-0734 PMID: 15525671

67. Bertin A., McMurray M. A., Pierson J., Thai L., McDonald K. L., Zehr E. A., García G. 3rd, Peters P., Thorner J., & Nogales E. (2012) Three-dimensional ultrastructure of the septin filament network in Saccharomyces cerevisiae. *Molecular Biology of the Cell*, 23, 423–432. https://doi.org/10.1091/mbc.E11-10-0850 PMID: 22160597

68. Dolat L., Hunyara J. L., Bowen J. R., Karasmanis E. P., Elgawly M., Galkin V. E., & Spiliotis E. T. (2014). Septins promote stress fiber–mediated maturation of focal adhesions and renal epithelial motility. *Journal of Cell Biology*, 207, 225–235. https://doi.org/10.1083/jcb.201405050 PMID: 25349260

69. Demmerle J., Innocent C., North A. J., Ball G., Müller M., Miron E., Matsuda A., Dobbie I. M., Markaki Y., & Schermelleh L. (2017). Strategic and practical guidelines for successful structured illumination microscopy. *Nature Prot*ocols, 12, 988–1010. https://doi.org/10.1038/nprot.2017.019 PMID: 28406496

70. Schermelleh L., Heintzmann R., & Leonhardt H. (2010). A guide to super-resolution fluorescence microscopy. *Journal of Cell Biology*, 190, 165–175. https://doi.org/10.1083/jcb.201002018 PMID: 20643879

71. Field C. M., Coughlin M., Doberstein S., Marty T., & Sullivan W. (2005). Characterization of anillin mutants reveals essential roles in septin localization and plasma membrane integrity. *Development*, 132, 2849–2860. https://doi.org/10.1242/dev.01843 PMID: 15930114

72. Zhao W. M., & Fang G. (2005). Anillin is a substrate of anaphase-promoting complex/cyclosome (APC/C) that controls spatial contractility of myosin during late cytokinesis. *Journal of Biology Chemistry*, 280, 33516–33524. https://doi.org/10.1074/jbc.M504657200 PMID: 16040610

73. Liu J., Fairn G. D., Ceccarelli D. F., Sicheri F., & Wilde A. (2012). Cleavage furrow organization requires PIP(2)-mediated recruitment of anillin. *Current Biology*, 22, 64–69. https://doi.org/10.1016/j.cub.2011.11.040 PMID: 22197245

74. Renshaw M. J., Liu J., Lavoie B. D., & Wilde A. (2014). Anillin-dependent organization of septin filaments promotes intracellular bridge elongation and Chmp4B targeting to the abscission site. *Open Biology*, 4, 130190. https://doi.org/10.1098/rsob.130190 PMID: 24451548

75. Bahler J., Steever A. B., Wheatley S., Wang Y., Pringle J. R., Gould K. L., & McCollum D. (1998). Role of polo kinase and Mid1p in determining the site of cell division in fission yeast. *Journal of Cell Biology*, 143, 1603–1616. https://doi.org/10.1083/jcb.143.6.1603 PMID: 9852154

76. McDonald N. A., Lind A. L., Smith S. E., Rong L., & Gould K. L. (2017). Nanoscale architecture of the *Schizosaccharomyces pombe* contractile ring. *eLife*, 6, e28865. https://doi.org/10.7554/eLife.28865 PMID: 28914606

77. Hartwell L. H. (1971). Genetic control of the cell division cycle in yeast. IV. Genes controlling bud emergence and cytokinesis. *Experimental Cell* Research, 69, 265–276. https://doi.org/10.1016/0014-4827(71)90223-0 PMID: 4950437

78. Joo E., Surka M. C., & Trimble W. S. (2007). Mammalian SEPT2 is required for scaffolding nonmuscle myosin II and its kinases. *Developmental Cell*, 13, 677–690. https://doi.org/10.1016/j.devcel.2007.09.001 PMID: 17981136

79. Bridges A. A., Zhang H., Mehta S. B., Occhipinti P., Tani T., & Gladfelter A. S. (2014). Septin assemblies form by diffusion-driven annealing on membranes. *Proceedings of the National Academy of Sciences USA*, 111, 2146–2151. https://doi.org/10.1073/pnas.1314138111 PMID: 24469790

80. Mavrakis M., Azou-Gros Y., Tsai F-C., Alvarado J., Bertin A., Iv F., Kress A., Brasselet S., Koenderink G. H., & Lecuit T. (2014). Septins promote F-actin ring formation by crosslinking filaments into curved bundles. *Nature Cell Biology*, 16, 322–334. https://doi.org/10.1038/ncb2921 PMID: 24633326

81. Etsey M. P., Di Ciano-Oliveira C., Froese C. D., Bejide M., & Trimble W. S. (2010). Distinct roles of septins in cytokinesis: SEPT9 mediates midbody abscission. *Journal Cell Biology*, 191, 741–749. https://doi.org/https%3A//doi.org/10.1083/jcb.201006031 PMID: 21059847

82. Kechad A., Jananji S., Ruella Y., & Hickson G. R. (2012). Anillin acts as a bifunctional linker coordinating midbody ring biogenesis during cytokinesis. *Current Biology*, 22, 197–203. https://doi.org/10.1016/j.cub.2011.11.062 PMID: 22226749

83. El Amine N., Kechad A., Jananji S., & Hickson G. R. (2013). Opposing actions of septins and Sticky on anillin promote the transition from contractile to midbody ring. *Journal of Cell Biology*, 203, 487–504. https://doi.org/10.1083/jcb.201305053 PMID: 24217622

84. Karasmanis E. P., Hwang D., Nakos K., Bowen J. R., Angelis D., & Spiliotis E. T. (2019). A septin double ring controls the spatiotemporal organization of the ESCRT machinery in cytokinetic abscission. *Current Biology*, 29, 2174–2182. https://doi.org/10.1016/j.cub.2019.05.050 PMID: 31204162